広島大学学位請求論文

Study of Chemical Potential Effects on Hadron by Lattice QCD

（ハドロンに対する化学ポテンシャルの効果の格子 QCD による研究）

2001 年

広島大学大学院理学研究科 物理科学 専攻

劉（リュウ） 玉斌（ユウビン）

Study of Chemical Potential Effects on Hadron by Lattice QCD

Yubin Liu

Departement of Physics, Hiroshima University,

Kagamiyama, Higashi-Hiroshima, 739-8521 Japan

Acknowledgments

I am grateful to my advisor, mentor, and collaborator Professor Osamu Miyamura. His enthusiasm for the subject and confidence in his insights have always motivated me to find the unknown and the inner laws of nature. Over these three years, he taught me the ways of thinking in lattice QCD, simulation methods, and many other things. Unfortunately he passed away on 10 July 2001. I will remember forever what we discussed in his last time in the hospital. His memory will always live.

I would like to thank Professor A .Nakamura (*Hiroshima University, Japan*), Professor T. Takaishi (*Hiroshima University of Economics, Japan*), and Dr. S. Choe (*Hiroshima University, Japan*) for useful comments and discussions. I have also benefited a lot from other members of QCD-TARO collaboration, especially, Ph. de Forcrand (*ETH-Hönggerberg*), M. García Pérez (*Theory Division, CERN*), H. Matsufuru (*Kyoto University*), and I.-O. Stamatescu (*Universität Heidelberg*), who checked my results and gave me helpful comments.

On 26-28 February 2001, a QCD-TARO collaboration meeting held in Hiroshima university. We also had an informal meeting in Humboldt university on 20 August 2001 during the Lattice 2001. In these meetings I discussed this work with our members. Their ideas and comments were very important for me to complete this work. Over the past three years, I have benefitted greatly from discussions with Professor A .Nakamura and Professor T. Takaishi. Their guidance has helped me to understand finite density study in lattice QCD which is difficult to present in monograph paper. Dr. S. Choe proved many results of this work from his side. Dr. H. Matsufuru came to my laboratory from Kyoto and gave me help when I needed. We discussed physics from late night till morning.

Finally, I want to express my gratitude to my wife and daughter for their love and patience. They always made me feel I could do it, and pushed me to do my best.

The Simulations in this work were performed on the HITACHI SR8000 at Information

Media Center (IMC), Hiroshima University, and on the NEC SX-5 at Institute for Nonlinear Sciences and Applied Mathematics (INSAM), Hiroshima University. I would also like to thank the staffs for supporting me.

Abstract

A formulation to obtain the response of hadron masses to the chemical potential is developed on the lattice. As a first trial, screening masses of pseudoscalar and vector mesons and their responses are evaluated. We present results on a $16 \times 8^2 \times 4$ lattice with $N_f = 2$ staggered fermions below and above T_c. The responses to both the isoscalar and isovector chemical potentials are sizable and they show different behaviors in low and high temperature phases, which may be a consequence of chiral symmetry restoration. We also measure the response of chiral condensate to chemical potential. The first and second responses of chiral condensate are evaluated. In both low and high temperature phase, the second responses are negative. They show that the transition point between chiral symmetry broken and chiral symmetry restoration phases decreases when chemical potential increases.

Contents

Chapter 1

Introduction

It is well established that Quantum Chromodynamics (QCD) is an underlying theory of strong interaction. This theory is formulated in terms of quarks and gluons which we believe are the basic degrees of freedom that make up hadronic matter. QCD has been very successful in predicting phenomena involving large momentum transfer. In this regime the coupling constant is small and perturbation theory becomes a reliable tool. On the other hand, at the scale of the hadronic world, the coupling constant is of order unity and perturbative methods fail. In this domain lattice QCD provides a non-perturbative tool for calculating the hadronic spectrum and the matrix elements of any operator within these hadronic states from first principles.

Good knowledge of QCD in the regime of finite temperature and baryon density is crucial for understanding a wide range of physical phenomena. In cosmology, one faces the problem of understanding how the universe has evolved through the QCD phase transition at temperature $T \sim 170$ MeV. Due to the smallness of the baryon asymmetry, finite temperature QCD should be sufficient to deal with this problem. On the other hand, neutron stars require the knowledge of matter in the dense regime, *i.e.*, at large baryon density and very low temperature[1]. Much less is known about the regime compared to that of high temperature baryon antibaryon symmetric QCD.

The numerical analysis of regularized filed theories can provide quantitative results on fundamental non-perturbative properties of QCD. It has been realized that this approach

[1] In this limit, quark matter is expected to behave as a color superconductor [1, 2].

will also allow to study the QCD phase transition and the equation of state of the quark-gluon plasma (QGP), and can also be used to address issues like the mechanism for confinement and chiral symmetry breaking, the role of topology, and the equilibrium properties of QCD at finite temperature [2]. Lattice QCD is QCD formulated on a discrete Euclidean space time grid. Since no new parameters or field variables are introduced in this discretization, lattice QCD retains the fundamental character of QCD. Input parameters in lattice simulations are coupling constant and the bare masses of quarks. Our belief is that these parameters are prescribed by some yet more fundamental underlying theory. However within the context of the standard model they have to be fixed in terms of an equal number of experimental quantities. This is what is done in lattice QCD. Therefore, if QCD is the correct theory of strong interactions, all predictions of lattice QCD have to match experimental data. A very useful feature of lattice QCD is that one can dial the input parameters. Therefore, in addition to testing QCD we can make detailed predictions of the dependence of quantities on coupling constants and the quark masses.

During the last two decades a lot of calculations about the phase structure of QCD at finite temperature have been carried out. In fact, we do understand quite well thermodynamics in the heavy quark mass limit of QCD, the pure SU(3) gauge theory, and even have calculated the critical temperature. Studies of such finite temperature transitions in QCD have made substantial progress, especially with the recent development of numerical algorithms for dynamical quarks in the simulation.

Most of the underlying physics of the QGP can be studied theoretically and computationally by lattice QCD. It has been quite successful in describing the physics at finite temperature with zero density. However, it is well known that studying finite density QCD through lattice simulations is a very hard problem. The fermionic determinant at finite chemical potential is complex, and gives an oscillating behavior in quantum averages which makes simulations very inefficient (see Appendix A.1). One can avoid this difficulty by considering SU(2) lattice QCD [5] which keeps action real even with chemical potential [3]. On the other hand, since the naive quenched approximation at finite chemical

[2] The breakthrough came with the lattice formulations of QCD by K. G. Wilson in 1974 [3]. The first numerical results on SU(2) pure gauge theory were presented by M. Creutz in 1980 [4].

[3] Note that the first lattice results in SU(2) QCD with finite chemical potential were reported by A. Nakamura almost two decades ago [6].

potential leads to an essentially different world [7], the use of dynamical fermions would be essential to extract the relevant physics. In spite of these difficulties, the study of hadrons in a finite baryonic environment is quite important [8, 9, 10], in view of recent experimental developments and of the theoretical interest in the phase structure of QCD. Search for the quark gluon plasma phase in high energy heavy ion collision experiments requires theoretical understanding of hadronic properties at finite temperature and density [11, 12]. Moreover, some experimental results can be interpreted by assuming a shift in the mass and the width of the ρ meson, induced by the dense nuclear medium even below the deconfinement transition [13, 14, 15].

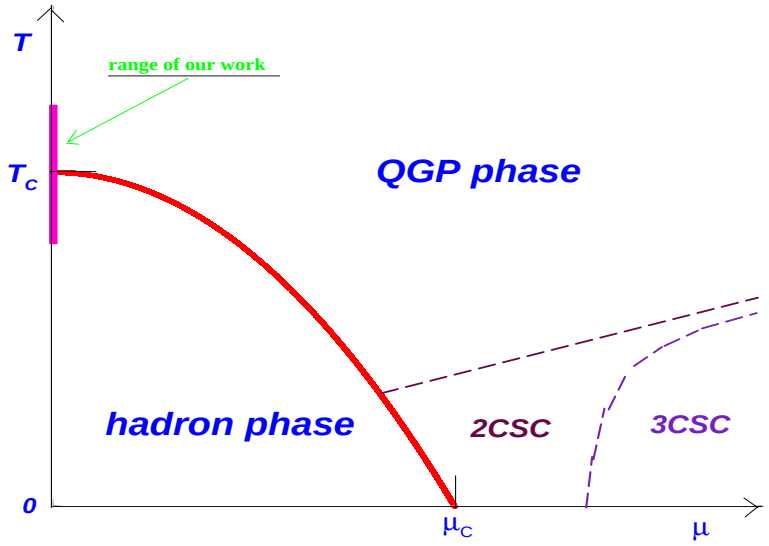

Figure 1.1: A schematic representation of a possible QCD phase diagram. At high temperature and density, matter is believed to be in QGP phase. The hadronic phase lies in the low temperature and density. At very high density but low temperature, when nuclei melt into each other, it has been suggested that a color superconductive phase might set in. $2CSC$ denotes a 2 flavor color superconductive regime. $3CSC$ is the 3 flavor regime. Our work range is around critical temperature at zero chemical potential.

In this study, we propose a new technique to investigate non-zero chemical potential using lattice QCD simulations. There are several approaches to circumvent the difficulty of studying a finite chemical potential system, and they seem successful to a limited extent [16, 17, 18, 19, 20]. In particular, the study of baryon number susceptibility at zero baryon density has reported an abrupt jump at the transition temperature [21, 22, 23]. There is in fact much interesting physical information which can be extracted from the behavior of a system at small chemical potential.

Our strategy is to expand the hadronic quantities, such as masses and chiral condensate, in the vicinity of zero chemical potential at finite temperature, and explore their changes through the response to the chemical potential at $\mu = 0$. An operator, ϑ, can be expanded in non-singular regions as

$$\vartheta|_\mu = \vartheta|_{\mu=0} + \mu \left.\frac{\partial \vartheta}{\partial \mu}\right|_{\mu=0} + \frac{1}{2}\mu^2 \left.\frac{\partial^2 \vartheta}{\partial \mu^2}\right|_{\mu=0} + O\left[\mu^3\right] \quad , \tag{1.0.1}$$

The first and the second derivatives of interesting observables with respect to chemical potential allows to perform the numerical simulations with standard methods [4]. The Taylor expansion in μ has also been used, and its properties discussed, in [20]. There, the behavior of observables, measured by standard methods as a function of an imaginary chemical potential μ, is fitted by a Taylor series amenable to analytic continuation to real μ (assuming a large enough analyticity domain). Here we measure the Taylor coefficients directly, in a single simulation, at $\mu = 0$, by calculating the derivatives of the relevant observables. Although the Taylor expansion cannot reproduce the non-analyticity inherent to a phase transition, it may suffice for observing the rounded, analytic behavior indicative of a phase transition in a finite volume, and for applying finite size scaling to probe the transition in the infinite volume limit.

We also measure the response of chiral condensate to the chemical potential. Studying for sufficiently light quark masses (such as u and d quarks) on lattice QCD at finite temperature with zero chemical potential, we can find a first order phase transition between a low temperature phase in which chiral symmetry is spontaneously broken and a high temperature phase in which chiral symmetry is restored [21, 22, 23]. Our preliminary results for response of hadron masses and chiral condensate have been reported in [26, 27, 28, 29, 30, 31].

The organization of this paper is as follows. In Chapter 2, we develop basic formulas to evaluate the first and second responses of hadron masses (Chapter 2.1) with respect to both isoscalar (Chapter 2.2) and isovector (Chapter 2.3) chemical potentials. In Chapter 2.4, we focus on the responses for $N_f = 2$ staggered fermion.

We study the responses of chiral condensate in Chapter 3. We also consider the isoscalar channel (Chapter 3.2) and isovector channel (Chapter 3.3) for the responses.

[4] for instance hybrid molecular dynamics algorithms [24], or hybrid Monte Carlo algorithms [25].

In Chapter 4, we present our numerical results. We explain details of responses for the pseudoscalar meson in the isoscalar channel (Chapter 4.2) and the isovector channel (Chapter 4.3). Study for vector meson is rather difficult. We show our preliminary results for the vector meson with the isoscalar and isovector chemical potentials in Chapter 4.4. The numerical results for chiral condensate will be discussed in Chapter 4.5. Numerical results are performed on a lattice of size $16 \times 8 \times 8 \times 4$ with standard Wilson gauge action and with two dynamical flavors of staggered quarks.

Chapter 2

Chemical potential responses for hadron masses

As we know the simulation of finite density system is difficult by lattice QCD approach. We turn to examine the response to the chemical potential for the hadronic mass and couplings in this chapter. Using a Taylor expansion method, at fixed temperature T and bare quark masses, the screening mass of a hadron is expanded in the form:

$$\left.\frac{M(\mu)}{T}\right|_{\mu} = \left.\frac{M}{T}\right|_{\mu=0} + \left(\frac{\mu}{T}\right)\left.\frac{\partial M}{\partial \mu}\right|_{\mu=0} + \left(\frac{\mu}{T}\right)^2 \frac{T}{2}\left.\frac{\partial^2 M}{\partial \mu^2}\right|_{\mu=0} + O\left[\left(\frac{\mu}{T}\right)^3\right] \quad , \qquad (2.0.1)$$

We can measure the first and the second derivatives of hadronic screening mass by standard simulation methods on lattice simulation. Using Eq. (2.0.1) the behavior of hadron at a small chemical potential will be obtained.

This Chapter is organized as follows. In section 2.1, we examine the basic formulas to evaluate the first and second responses of hadronic screening mass with respect to chemical potential from hadron correlator function. The chemical potential will be chosen two types, *i.e.*, isoscalar chemical potential ($\mu_S = \mu_u = \mu_d$) and isovector chemical potential ($\mu_V = \mu_u = -\mu_d$). We give the details of the formulas for the isoscalar response in section 2.2, and those for isovector case in section 2.3. In section 2.4, we focus on the expression of using staggered fermion action.

2.1 The response of hadron masses to the chemical potential

This section develops the basic framework to observe the response of hadron masses with respect to the chemical potential. The basic framework is as follows. Suppose that a hadron correlator is dominated by a single pole[1]

$$C(x) = \sum_{y,z,t} \langle H(x,y,z,t) H(0,0,0,0)^\dagger \rangle = \frac{\hat{\gamma}}{2\hat{M}} \left(e^{-\hat{M}\hat{x}} + e^{-\hat{M}(L_x - \hat{x})} \right) \quad , \tag{2.1.1}$$

where $\hat{M} = aM$ and $\hat{x} = \frac{x}{a}$ [2]. L_x is the lattice size of x-direction. $\hat{\gamma}$ is the residue appeared in the propagator as $\frac{\gamma}{(p^2+m^2)}$, and it is better to consider genuine coupling of the hadronic pole. In the following, we write $A = \frac{\hat{\gamma}}{2\hat{M}}$. The value of A depends on the choice of sources. But its behavior as a function of the chemical potential provides information on the coupling to medium. We take the first and the second derivatives with respect to $\hat{\mu} \equiv a_t \mu = \frac{\mu}{(N_t T)}$ where μ is the chemical potential;

$$C(x)^{-1} \frac{\partial C(x)}{\partial \hat{\mu}} = A^{-1} \frac{\partial A}{\partial \hat{\mu}} + \frac{\partial \hat{M}}{\partial \hat{\mu}} \left[\left(\hat{x} - \frac{L_x}{2} \right) \tanh \left\{ \hat{M} \left(\hat{x} - \frac{L_x}{2} \right) \right\} - \frac{L_x}{2} \right] \tag{2.1.2}$$

and

$$\begin{aligned} C(x)^{-1} \quad & \frac{\partial^2 C(x)}{\partial \hat{\mu}^2} = A^{-1} \frac{\partial^2 A}{\partial \hat{\mu}^2} \\ + \quad & \left(2A^{-1} \frac{\partial A}{\partial \hat{\mu}} \frac{\partial \hat{M}}{\partial \hat{\mu}} + \frac{\partial^2 \hat{M}}{\partial \hat{\mu}^2} \right) \left[\left(\hat{x} - \frac{L_x}{2} \right) \tanh \left\{ \hat{M} \left(\hat{x} - \frac{L_x}{2} \right) \right\} - \frac{L_x}{2} \right] \\ + \quad & \left(\frac{\partial \hat{M}}{\partial \hat{\mu}} \right)^2 \left[\left(\hat{x} - \frac{L_x}{2} \right)^2 + \frac{L_x^2}{4} - L_x \left(\hat{x} - \frac{L_x}{2} \right) \tanh \left\{ \hat{M} \left(\hat{x} - \frac{L_x}{2} \right) \right\} \right] \quad . \end{aligned} \tag{2.1.3}$$

$C(x)$ and the first and the second derivatives of $C(x)$ are calculated from lattice simulations. Then, using the right-hand side of Eqs. (2.1.2) and (2.1.3), the first and the second responses of the hadron mass and coupling are determined.

Next problem is how to get the derivative of the correlator from lattice simulations. For this purpose, we go back to the definition of the hadron correlator. In this work, we treat flavor non-singlet mesons in two flavor QCD. The hadron correlator is given by

$$\langle H(n) H(0)^\dagger \rangle = \langle G \rangle \quad , \tag{2.1.4}$$

[1] Generalization to a multi-pole fit is strait forward.

[2] The mass parameter M and space-time vector x are according to their "canonical" dimension, a is lattice spacing taking the dimension of length, $\hat{M}$ and $\hat{x}$ are dimensionless quantities.

where G is the meson propagator part

$$G = \mathrm{Tr}\left[g\left(\hat{\mu}_u\right)_{n:0} \Gamma g\left(\hat{\mu}_d\right)_{0:n} \Gamma^\dagger \right] \quad . \tag{2.1.5}$$

Here $g(\hat{\mu})$ is the quark propagator at finite chemical potential, and Γ is the Dirac matrix which specifies the spin of the meson. The quark propagator is related to the Dirac operator $D[U;\hat{\mu}]$ in the background gauge field configuration U as

$$g(\hat{\mu}) = D(\hat{\mu})^{-1}. \tag{2.1.6}$$

$\langle O \rangle$ means

$$\langle O \rangle = \frac{\int [dU]\, O \Delta e^{-S_G}}{\int [dU]\, \Delta e^{-S_G}} \quad , \tag{2.1.7}$$

where S_G is the gluonic action and Δ is the fermion determinant,

$$\Delta = \prod_{i=1}^{N_f} \det\left(D\left(\hat{\mu}_i\right)\right) \quad , \tag{2.1.8}$$

for two light flavors fermion, i.e., $N_f = 2$. Δ can be written as

$$\Delta = \det(D(\hat{\mu}_u))\det(D(\hat{\mu}_d)) \quad . \tag{2.1.9}$$

Then, the first and the second derivatives are

$$\frac{\partial}{\partial \hat{\mu}} \langle H(n) H(0)^\dagger \rangle = \left\langle \dot{G} + G\frac{\dot{\Delta}}{\Delta} \right\rangle - \langle G \rangle \left\langle \frac{\dot{\Delta}}{\Delta} \right\rangle \tag{2.1.10}$$

and

$$\begin{aligned} \frac{\partial^2}{\partial \hat{\mu}^2} \langle H(n) H(0)^\dagger \rangle &= \left\langle \ddot{G} + 2\dot{G}\frac{\dot{\Delta}}{\Delta} + G\frac{\ddot{\Delta}}{\Delta} \right\rangle - 2\left\langle \dot{G} + G\frac{\dot{\Delta}}{\Delta} \right\rangle \left\langle \frac{\dot{\Delta}}{\Delta} \right\rangle \\ &- \langle G \rangle \left[\left\langle \frac{\ddot{\Delta}}{\Delta} \right\rangle - 2\left\{ \left\langle \frac{\dot{\Delta}}{\Delta} \right\rangle \right\}^2 \right] \quad , \end{aligned} \tag{2.1.11}$$

where the dots $\dot{O}$ and $\ddot{O}$ stand for the first and the second derivatives with respect to $\hat{\mu}$ of an operator O.

At zero chemical potential, we have simpler expressions since

$$\left\langle \frac{\dot{\Delta}}{\Delta} \right\rangle = 0 \quad \text{for} \quad \hat{\mu} = 0 \quad . \tag{2.1.12}$$

Eq. (2.1.12) corresponds to the fact that the average baryon number density is zero at $\hat{\mu}=0$. Actually, we see that $\frac{\partial \det(D)}{\partial \hat{\mu}} = \mathrm{Tr}\left[\dot{D}D^{-1}\right]\det(D)$ is anti-hermitian at $\hat{\mu}=0$:

$$\mathrm{Tr}\left[\dot{D}D^{-1}\right] = \mathrm{Tr}\left[\dot{D}\gamma_5\gamma_5 D^{-1}\right] = -\mathrm{Tr}\left[\gamma_5\dot{D}^\dagger(D^\dagger)^{-1}\gamma_5\right] = -\mathrm{Tr}\left[\dot{D}D^{-1}\right]^* \ . \quad (2.1.13)$$

This means that $\frac{\partial \det(D)}{\partial \hat{\mu}}$ changes sign under the transformation $U \to U^\dagger$. Since the measure and the gluonic action are invariant in this transformation, its expectation value vanishes[21]. Thus, at zero chemical potential, Eqs. (2.1.10) and (2.1.11) turn to

$$\begin{aligned} \frac{\partial}{\partial\hat{\mu}}\langle H(n)H(0)^\dagger\rangle &= \left\langle \dot{G} + G\frac{\dot{\Delta}}{\Delta}\right\rangle \ , \quad (2.1.14)\\ \frac{\partial^2}{\partial\hat{\mu}^2}\langle H(n)H(0)^\dagger\rangle &= \left\langle \ddot{G} + 2\dot{G}\frac{\dot{\Delta}}{\Delta} + G\frac{\ddot{\Delta}}{\Delta}\right\rangle - \langle G\rangle\left\langle\frac{\ddot{\Delta}}{\Delta}\right\rangle \ . \end{aligned}$$

2.2 Formulas for the isoscalar response

We investigate derivatives with respect to both isoscalar and isovector types of chemical potential. The isoscalar chemical potential corresponds to the quark number. In this section we study the isoscalar chemical potential (in the next section we will study behavior of isovector type) response by setting

$$\hat{\mu}_S = \hat{\mu}_u = \hat{\mu}_d \ . \quad (2.2.1)$$

The first and the second derivatives of correlator with respect $\hat{\mu}$ are given by fermion operators

$$\frac{\partial}{\partial\hat{\mu}}\mathrm{Re}\langle H(n)H(0)^\dagger\rangle = 0 \ , \quad (2.2.2)$$

and

$$\begin{aligned} \frac{\partial^2}{\partial\hat{\mu}^2} \ \mathrm{Re} \ & \langle H(n)H(0)^\dagger\rangle = 4\mathrm{Re}\left\langle \mathrm{Tr}\left[\left(g\dot{D}g\dot{D}g\right)_{n:0}\Gamma\gamma_5 g^\dagger_{n:0}\gamma_5\Gamma^\dagger\right]\right\rangle \quad (2.2.3)\\ & - 2\mathrm{Re}\left\langle \mathrm{Tr}\left[\left(g\ddot{D}g\right)_{n:0}\Gamma\gamma_5 g^\dagger_{n:0}\gamma_5\Gamma^\dagger\right]\right\rangle \\ & - 2\mathrm{Re}\left\langle \mathrm{Tr}\left[\left(g\dot{D}g\right)_{n:0}\Gamma\gamma_5\left(g\dot{D}g\right)^\dagger_{n:0}\gamma_5\Gamma^\dagger\right]\right\rangle \\ & + 8\left\langle \mathrm{ImTr}\left[\left(g\dot{D}g\right)_{n:0}\Gamma\gamma_5 g^\dagger_{n:0}\gamma_5\Gamma^\dagger\right]\mathrm{ImTr}\left[\dot{D}g\right]\right\rangle \\ & + 2\mathrm{Re}\left\{\left\langle \mathrm{Tr}\left[g_{n:0}\Gamma\gamma_5 g^\dagger_{n:0}\gamma_5\Gamma^\dagger\right]\left(\mathrm{Tr}\left[\ddot{D}g\right] - \mathrm{Tr}\left[\dot{D}g\dot{D}g\right] + 2\mathrm{Tr}\left[\dot{D}g\right]^2\right)\right\rangle\right. \\ & - \left.\left\langle \mathrm{Tr}\left[g_{n:0}\Gamma\gamma_5 g^\dagger_{n:0}\gamma_5\Gamma^\dagger\right]\right\rangle\left\langle \mathrm{Tr}\left[\ddot{D}g\right] - \mathrm{Tr}\left[\dot{D}g\dot{D}g\right] + 2\mathrm{Tr}\left[\dot{D}g\right]^2\right\rangle\right\}. \end{aligned}$$

2.3 Formulas for the isovector response

In this section, we study the case of isovector chemical potential type. The isovector chemical potential is defined as

$$\hat{\mu}_V = \hat{\mu}_u = -\hat{\mu}_d \quad . \tag{2.3.1}$$

Note that Son and Stephanov proposed a model corresponding to the isovector case as a good test bed for the chemical potential problem [32]. We can find the first and the second responses for isovector chemical potential as

$$\frac{\partial}{\partial\hat{\mu}}\mathrm{Re}\langle H(n)H(0)^\dagger\rangle = -2\mathrm{ReTr}\left[\left(g\dot{D}g\right)_{n:0}\Gamma\gamma_5 g^\dagger_{n:0}\gamma_5\Gamma^\dagger\right] \quad , \tag{2.3.2}$$

and

$$\begin{aligned}\frac{\partial^2}{\partial\hat{\mu}^2}\mathrm{Re}\langle H(n)H(0)^\dagger\rangle &= 4\mathrm{Re}\left\langle \mathrm{Tr}\left[\left(g\dot{D}g\dot{D}g\right)_{n:0}\Gamma\gamma_5 g^\dagger_{n:0}\gamma_5\Gamma^\dagger\right]\right\rangle \\ &- 2\mathrm{Re}\left\langle \mathrm{Tr}\left[\left(g\ddot{D}g\right)_{n:0}\Gamma\gamma_5 g^\dagger_{n:0}\gamma_5\Gamma^\dagger\right]\right\rangle \\ &+ 2\mathrm{Re}\left\langle \mathrm{Tr}\left[\left(g\dot{D}g\right)_{n:0}\Gamma\gamma_5\left(g\dot{D}g\right)^\dagger_{n:0}\gamma_5\Gamma^\dagger\right]\right\rangle \\ &+ 2\mathrm{Re}\left\{\left\langle \mathrm{Tr}\left[g_{n:0}\Gamma\gamma_5 g^\dagger_{n:0}\gamma_5\Gamma^\dagger\right]\left(\mathrm{Tr}\left[\ddot{D}g\right]-\mathrm{Tr}\left[\dot{D}g\dot{D}g\right]\right)\right\rangle\right. \\ &- \left.\left\langle \mathrm{Tr}\left[g_{n:0}\Gamma\gamma_5 g^\dagger_{n:0}\gamma_5\Gamma^\dagger\right]\right\rangle\left\langle \mathrm{Tr}\left[\ddot{D}g\right]-\mathrm{Tr}[\dot{D}g\dot{D}g]\right\rangle\right\} \quad .\end{aligned} \tag{2.3.3}$$

2.4 The response formulas for using $N_f = 2$ staggered fermion

Our simulations with $N_f = 2$ dynamical quarks are performed by using staggered fermion. The fermion operator and its derivatives are

$$\begin{aligned}D(U,\hat{\mu})_{n,m} &= ma\delta_{n,m} + \frac{1}{2}\sum_{\sigma=x,y,z}\eta_\sigma(n)\left[U_{\hat{\sigma}}(n)\delta_{n+\hat{\sigma},m} - U^\dagger_{\hat{\sigma}}(n-\hat{\sigma})\delta_{n-\hat{\sigma},m}\right] \\ &+ \frac{1}{2}\eta_t(n)\left[U_{\hat{t}}(n)e^{\hat{\mu}}\delta_{n+\hat{t},m} - U^\dagger_{\hat{t}}(n-\hat{t})e^{-\hat{\mu}}\delta_{n-\hat{t},m}\right] \quad ,\end{aligned} \tag{2.4.1}$$

$$\frac{\partial D}{\partial\hat{\mu}} = \frac{1}{2}\eta_t(n)\left[U_{\hat{t}}(n)e^{\hat{\mu}}\delta_{n+\hat{t},m} + U^\dagger_{\hat{t}}(n-\hat{t})e^{-\hat{\mu}}\delta_{n-\hat{t},m}\right] \quad , \tag{2.4.2}$$

and

$$\frac{\partial^2 D}{\partial\hat{\mu}^2} = \frac{1}{2}\eta_t(n)\left[U_{\hat{t}}(n)e^{\hat{\mu}}\delta_{n+\hat{t},m} - U^\dagger_{\hat{t}}(n-\hat{t})e^{-\hat{\mu}}\delta_{n-\hat{t},m}\right] \quad , \tag{2.4.3}$$

where $\hat{\sigma}$ and $\hat{t}$ are unit vectors pointing along the space and time directions.

We take into account the four fold degeneracy of the staggered fermion operator. Meson operator is

$$G = \mathrm{Tr}\left[g(\hat{\mu}_S)g^\dagger(-\hat{\mu}_S)\cdot\boldsymbol{\sigma}\right] \tag{2.4.4}$$

for isoscalar chemical potential, where $\boldsymbol{\sigma}$ means

$$\boldsymbol{\sigma} = 1 \qquad for\ pseudoscalar\ meson \tag{2.4.5}$$

$$\boldsymbol{\sigma} = (-1)^{ny} + (-1)^{nz} + (-1)^{nt} \qquad for\ vector\ meson\ . \tag{2.4.6}$$

For the isovector chemical potential

$$G = \mathrm{Tr}\left[g(\hat{\mu}_V)g^\dagger(-\hat{\mu}_V)\cdot\boldsymbol{\sigma}\right] \tag{2.4.7}$$

The determinant factor Δ of $N_f = 2$ fermions is

$$\Delta = \exp\left[\frac{1}{4}\mathrm{Trln}D(U,\hat{\mu}_u) + \frac{1}{4}\mathrm{Trln}D(U,\hat{\mu}_d)\right] \quad . \tag{2.4.8}$$

Further details of the first and the second derivatives of the hadron correlator with respect to $\hat{\mu}$ will be given by fermion operators in Appendix. For the isoscalar (isovector) potential response, we will give concrete formulae in Appendix B.1 (C.1). In Appendix D.1 we show them explicitly for the staggered fermion action.

Chapter 3

The response of chiral condensate

For the response of chiral order parameter $\langle\bar{\psi}\psi\rangle$ with respect to the chemical potential at finite temperature, we use a similar method in Chapter 2, Using a Taylor expansion method, at fixed temperature T and bare quark masses, we can expand $\langle\bar{\psi}\psi\rangle$ as:

$$\begin{aligned}\frac{\langle\bar{\psi}\psi\rangle(\mu)}{T^3}\Big|_{\mu} &= \frac{\langle\bar{\psi}\psi\rangle}{T^3}\Big|_{\mu=0} + \left(\frac{\mu}{T}\right)\frac{1}{T^2}\,\frac{\partial\langle\bar{\psi}\psi\rangle}{\partial\mu}\Big|_{\mu=0} \\ &+ \left(\frac{\mu}{T}\right)^2\frac{1}{2T}\,\frac{\partial^2\langle\bar{\psi}\psi\rangle}{\partial\mu^2}\Big|_{\mu=0} + O\left[\left(\frac{\mu}{T}\right)^3\right] \quad . \end{aligned} \tag{3.0.1}$$

The $\frac{\partial\langle\bar{\psi}\psi\rangle}{\partial\mu}\Big|_{\mu=0}$ and $\frac{\partial^2\langle\bar{\psi}\psi\rangle}{\partial\mu^2}\Big|_{\mu=0}$ can be obtained by numerical simulation. Using Eq. (3.0.1), we can investigate the behavior of $\langle\bar{\psi}\psi\rangle$ at a small chemical potential. It presents a new point of view for studying the transition between chiral symmetry broken phase and restored phase in finite fermion number density.

In this chapter, we discuss it in details. In section 3.1, we write down the the first and the section responses for $\langle\bar{\psi}\psi\rangle$. The formulas for isoscalar and isovector response are described in section 3.2 and section 3.3. Using two light flavors of staggered fermion, the response of $\langle\bar{\psi}\psi\rangle$ are appeared in Appendix D.1.2.

3.1 The chiral condensate response in lattice QCD

We go back to definition of the meson propagator. We treat flavor non-singlet mesons in two flavor QCD. In lattice QCD, chiral condensate can be written as

$$\langle\bar{\psi}\psi\rangle = \mathrm{Re}\langle G\rangle \quad . \tag{3.1.1}$$

For an expectation value of the observable G, the first and second responses to the chemical potential $\hat{\mu}$ at $\hat{\mu}=0$ are given by

$$\frac{\partial}{\partial\hat{\mu}}\langle G\rangle = \left\langle \dot{G} + G\frac{\dot{\Delta}}{\Delta}\right\rangle \tag{3.1.2}$$

$$\frac{\partial^2}{\partial\hat{\mu}^2}\langle G\rangle = \left\langle \ddot{G} + 2\dot{G}\frac{\dot{\Delta}}{\Delta}\right\rangle + \left\langle G\circ\frac{\ddot{\Delta}}{\Delta}\right\rangle_{cc} \quad , \tag{3.1.3}$$

where

$$\langle A\circ B\rangle_{cc} = \langle AB\rangle - \langle A\rangle\langle B\rangle \quad , \tag{3.1.4}$$

and Δ is given in Eq. (2.1.9). G is a trace of fermion propagator, and it is different for isoscalar and isovector chemical potential. [1]

3.2 Formulas for the isoscalar response

For response of the isoscalar chemical potential, we consider a trace of fermion propagator using Eq. (2.2.1),

$$G = \frac{1}{2}\left\{\mathrm{Tr}\left[g(\hat{\mu}_u)\right] + \mathrm{Tr}[g(\hat{\mu}_d)]\right\} = \mathrm{Tr}\left[g(\hat{\mu}_S)\right] \quad . \tag{3.2.1}$$

At $\hat{\mu}_S = 0$ the first and the second derivative are

$$\dot{G} = -\mathrm{Tr}\left[g\dot{D}g\right] \tag{3.2.2}$$

$$\ddot{G} = -\mathrm{Tr}\left[g\ddot{D}g\right] + 2\mathrm{Tr}\left[g\dot{D}g\dot{D}g\right] \quad . \tag{3.2.3}$$

[1] See Eq. (3.2.1) for isoscalar potential and Eq. (3.3.1) for isovector potential

Combining Eq. (3.1.2), Eq. (3.1.3), Eq. (B.1.9), Eq. (3.2.2) and Eq. (3.2.3) we have

$$\frac{\partial}{\partial\hat{\mu}}\mathrm{Re}\langle G\rangle = 0 \tag{3.2.4}$$

and

$$\begin{aligned}\frac{\partial^2}{\partial\hat{\mu}^2}\mathrm{Re}\langle G\rangle &= 2\mathrm{Re}\left\langle \mathrm{Tr}\left[g\dot{D}g\dot{D}g)\right]\right\rangle - \mathrm{Re}\left\langle \mathrm{Tr}[g\ddot{D}g]\right\rangle \\ &+ 4\left\langle \mathrm{ImTr}\left[g\dot{D}g\right]\mathrm{ImTr}\left[\dot{D}g\right]\right\rangle \\ &+ \left\langle \mathrm{ReTr}\left[g\right]\circ\left(2\mathrm{ReTr}\left[\ddot{D}g\right] - 2\mathrm{ReTr}\left[\dot{D}g\dot{D}g)\right] - 4\left\{\mathrm{ImTr}\left[\dot{D}g\right]\right\}^2\right)\right\rangle_{cc}\end{aligned} \tag{3.2.5}$$

3.3 Formulas for the isovector response

Since the isovector chemical potential is defined by Eq. (2.3.1), the trace of fermion propagator is

$$G = \frac{1}{2}\left\{\mathrm{Tr}\left[g(\hat{\mu}_u)\right] + \mathrm{Tr}\left[g(\hat{\mu}_d)\right]\right\} = \frac{1}{2}\left\{\mathrm{Tr}\left[g\left(\hat{\mu}\right)\right] + \mathrm{Tr}\left[g\left(-\hat{\mu}\right)\right]\right\} \tag{3.3.1}$$

Similarly, derivatives of G are calculated as

$$\dot{G} = 0 \tag{3.3.2}$$

$$\ddot{G} = -\mathrm{Tr}\left[g\ddot{D}g\right] + 2\mathrm{Tr}\left[g\dot{D}g\dot{D}g\right] \quad . \tag{3.3.3}$$

Combining Eq. (3.1.2), Eq. (3.1.3), Eq. (C.1.1), Eq. (C.1.2) Eq. (3.3.2) and Eq. (3.3.3) we have

$$\frac{\partial}{\partial\hat{\mu}}\mathrm{Re}\langle G\rangle = 0 \tag{3.3.4}$$

and

$$\begin{aligned}\frac{\partial^2}{\partial\hat{\mu}^2}\mathrm{Re}\langle G\rangle &= 2\mathrm{Re}\left\langle \mathrm{Tr}\left[g\dot{D}g\dot{D}g\right]\right\rangle - \mathrm{Re}\left\langle \mathrm{Tr}\left[g\ddot{D}g\right]\right\rangle \\ &+ \left\langle \mathrm{ReTr}\left[g\right]\circ\left\{2\mathrm{ReTr}\left[\ddot{D}g\right] - 2\mathrm{ReTr}\left[\dot{D}g\dot{D}g\right]\right\}\right\rangle_{cc}\end{aligned} \tag{3.3.5}$$

In Appendix B.1.2, C.1.2, and D.1.2, we also discuss responses of chiral condensate to the chemical potential using two light flavors of staggered fermion. We give formulas in Eq. (D.1.5) and Eq. (D.1.6) for the isoscalar chemical potential and the isovector chemical potential, respectively.

Chapter 4

Numerical results

4.1 Simulation parameters

ma	β	$\#conf.$	T/T_C
0.0125	5.26	1200	0.985
	5.34	600	1.098
0.0170	5.26	1200	0.977
	5.34	600	1.089
0.0250	5.20	1200	0.888
	5.26	1200	0.963
	5.28	600	0.990
	5.29	600	1.003
	5.30	300	1.017
	5.32	600	1.045
	5.34	600	1.074
	5.36	300	1.104
	5.40	300	1.165

Table 4.1: Parameters of the simulations. $\#conf.$ stands for the number of configurations analyzed.

In this study, simulations are done on a $16 \times 8^2 \times 4$ lattice. We take an interest in responses of hadrons below and above the confinement/deconfinement phase transition temperature. For two light flavors of staggered fermion, the critical coupling β_c is carried out at $N_t = 4$, i.e., $\beta_c = 5.271$ for $ma = 0.0125$, and $\beta_c = 5.288$ for $ma = 0.025$ [33, 34]. Our simulations are carried out with the R-algorithm. The time step of molecular dynamics is taken as $\delta = 0.01$. To evaluate the trace, 'Tr', the Z_2 noise method [35] is used,

and the number of noise vectors is two hundred [1] . Hadronic correlators are measured by using the corner-type wall source [22] after Coulomb gauge fixing in each x-plane, and we choose three quark masses, $ma = 0.0125$, 0.017, 0.025. The Wilson and Polyakov loop are shown in Fig. 4.1, and the chiral condensate for $ma = 0.025$ is shown in Fig. 4.2. The number of configurations used for calculations of the correlators is summarized in Table 4.1.

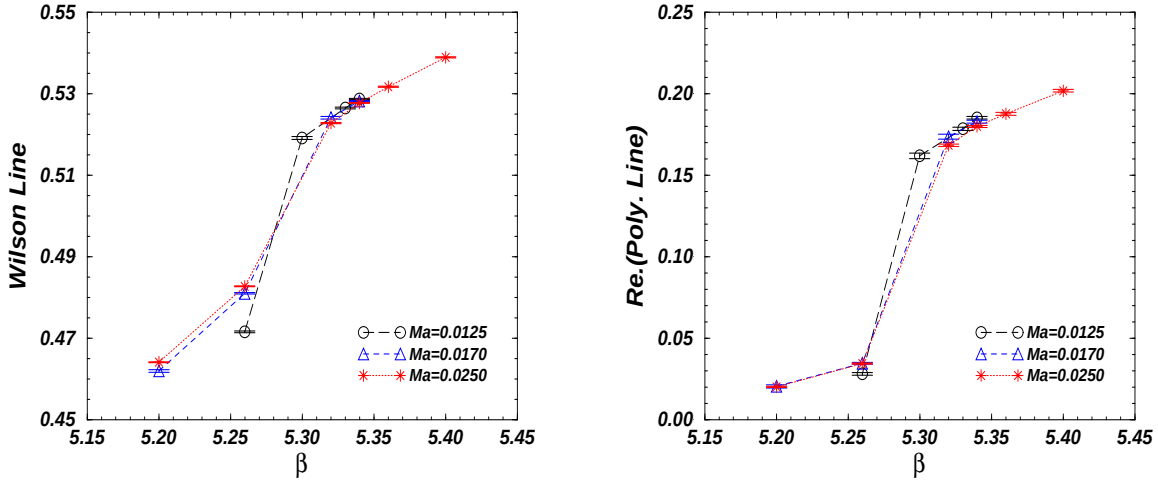

Figure 4.1: Average value of Wilson line (left figure) and Polyakov line (right figure) as a function of β.

The expressions of responses, Eqs. (2.3.2), (D.1.3), and (D.1.4) in Appendix, consist of many terms. We show typical features of the terms. As seen in Fig. 4.7, the pseudoscalar correlator is measured with very small error bars. Fitting by the single pole is very successful for an interval $1 < x/a < 15$.

$$
\begin{aligned}
(A) \quad &: \quad 2\sum_{y,z,t} \mathrm{Re}\left\langle \left| \left(g\dot{D}g\right)_{n:0} \right|^2 \right\rangle \\
(B) \quad &: \quad 4\sum_{y,z,t} \mathrm{Re}\left\langle \mathrm{Tr}\left[\left(g\dot{D}g\dot{D}g\right)_{n:0} g^{\dagger}_{n:0} \right] \right\rangle \\
(D) \quad &: \quad 2\sum_{y,z,t} \mathrm{Re}\left\langle \mathrm{Tr}\left[\left(g\ddot{D}g\right)_{n:0} g^{\dagger}_{n:0} \right] \right\rangle
\end{aligned}
\tag{4.1.1}
$$

are also presented in Fig. 4.4 $\sim$ Fig. 4.7. The figure shows that all the quantities are measurable with acceptable errors. We find that B and D term depend on coupling β,

[1] We study the relation between necessary terms and noise vectors in Appendix E.

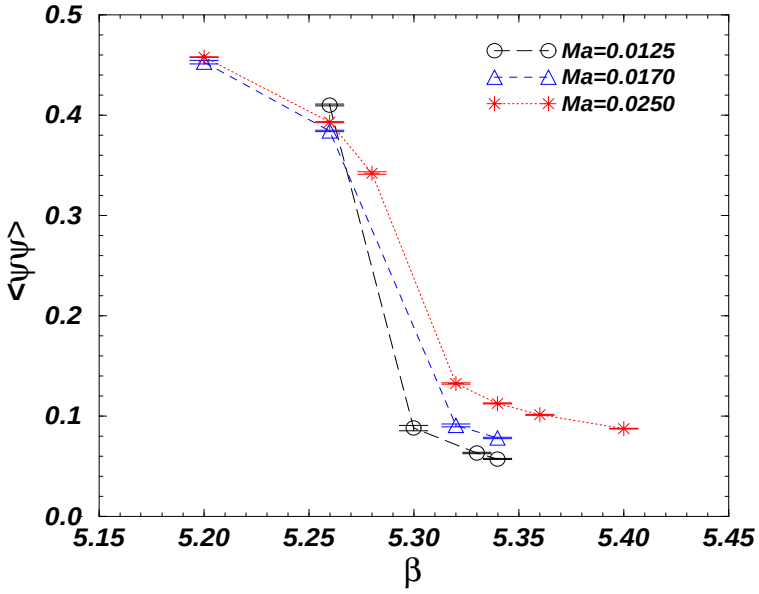

Figure 4.2: Average value of chiral condensate as a function of β.

and have

$$B\ term > D\ term \qquad below\ \beta_C$$

$$B\ term < D\ term \qquad above\ \beta_C$$

Fig. 4.8 $\sim$ Fig. 4.11 show $C^{-1}d^2C/d\hat{\mu}^2$ at $\beta = 5.26$ (below β_c) and 5.34 (above β_c) for the isoscalar and isovector chemical potentials. The solid curves are fittings by Eq. (2.1.3) and they describe the data reasonably well.

Let us turn to the first order response to the isovector chemical potential. Note that the first order response is identically zero. Fig. 4.12 $\sim$ Fig. 4.14 shows $C^{-1}dC/d\hat{\mu}_V$ at $\beta = 5.26$ and 5.34. Both data do not indicate sizable values for the first order response.

4.2 Responses of the pseudoscalar meson to the isoscalar chemical potential

We determine the response of a meson mass as follows. First we determine the meson mass $\hat{M}$ by a usual step. Namely, we fit the MC results of the correlator to Eq. (2.1.1). The value of the meson mass $\hat{M}$ is obtained as a fitting parameter. Then, substituting

ma	β	$\hat{M}$	$\frac{1}{A}\frac{d^2A}{d\hat{\mu}^2}$	$\frac{d^2\hat{M}}{d\hat{\mu}^2}$	$\frac{1}{\hat{\gamma}}\frac{d^2\hat{\gamma}}{d\hat{\mu}^2}$
0.0125	5.26	0.2956(2)	-1.4(20)	0.17(35)	-0.8(23)
	5.34	0.7513(11)	-4.23(49)	5.39(10)	2.95(51)
0.0170	5.26	0.3506(2)	-1.5(14)	0.30(26)	-0.6(16)
	5.34	0.7421(35)	-3.68(75)	5.82(16)	4.16(78)
0.0250	5.20	0.4061(2)	-0.4(14)	0.16(26)	0.0(16)
	5.26	0.4218(2)	-0.8(11)	0.29(20)	-0.1(12)
	5.28	0.4450(3)	-1.8(21)	1.36(39)	1.18(23)
	5.29	0.4861(3)	-8.6(8)	3.37(16)	-1.64(92)
	5.30	0.5956(8)	-5.8(10)	4.03(21)	0.9(10)
	5.32	0.6926(11)	-4.65(91)	5.17(20)	2.82(96)
	5.34	0.7534(7)	-3.17(41)	4.43(8)	2.71(42)
	5.36	0.7956(7)	-3.01(48)	4.89(1)	3.14(49)
	5.40	0.8600(6)	-1.83(38)	5.04(8)	4.02(38)

Table 4.2: Responses of the pseudoscalar meson to $\hat{\mu}_S$.

$\hat{M}$ to Eqs. (2.1.2) and (2.1.3), we fit the MC results of the first and second responses to these equations and obtain the responses as fitting parameters. Note that for $\hat{\mu}_S$ response we omit the fitting step to the first order response since it vanishes (see Eq. (2.2.2) in Appendix). Results of the pseudoscalar meson for the isoscalar chemical potential are summarized in Table 4.2. The screening mass of the pseudoscalar meson at $ma = 0.025$ as a function of T/T_c is shown in Fig. 4.16 .

In low temperature phase, the response of the mass is small. This behavior of the mass can be considered as the persistence of nature of Nambu-Goldstone boson. In fact, if the chiral extrapolation is made, the limiting value of the isoscalar response is consistent with zero as shown in Fig. 4.17. In addition, our results suggest that the response of the coupling is small below T_c.

Above T_c, we first note that the correlator and its response are still well fitted by single pole formulae, Eqs. (2.1.1-2.1.3). Screening masses are manifestly larger than those below T_c. This confirms the results of the previous work [23]. The pseudoscalar meson seems to be free from the nature of Nambu-Goldstone boson. The response of the mass above T_c becomes large. In the sense of the screening length, chemical potential effect enhances a shielding of the pseudoscalar charge. We also note that the response of the coupling increases.

ma	β	$\frac{1}{A}\frac{dA}{d\hat{\mu}}$	$\frac{d\hat{M}}{d\hat{\mu}}$	$\frac{1}{A}\frac{d^2A}{d\hat{\mu}^2}$	$\frac{d^2\hat{M}}{d\hat{\mu}^2}$	$\frac{1}{\hat{\gamma}}\frac{d^2\hat{\gamma}}{d\hat{\mu}^2}$
0.0125	5.26	0.0029(57)	-0.0001(12)	47.46(71)	-12.93(43)	3.7(16)
	5.34	0.0047(93)	0.0006(21)	2.32(64)	-1.32(32)	0.56(77)
0.0170	5.26	-0.0081(48)	-0.0005(10)	33.52(61)	-10.49(33)	3.6(11)
	5.34	0.0000(82)	-0.0012(19)	2.74(64)	-1.48(32)	0.75(78)
0.0250	5.20	0.0062(39)	0.0016(8)	25.24(46)	-9.10(23)	2.84(74)
	5.26	-0.0080(37)	0.0007(8)	23.22(46)	-8.64(23)	2.72(71)
	5.28	0.0047(55)	0.0010(12)	19.58(91)	-7.65(45)	2.4(14)
	5.29	0.0012(31)	0.0003(6)	12.43(70)	-5.48(35)	1.2(10)
	5.30	-0.013(7)	-0.0004(14)	6.99(99)	-3.74(50)	0.7(13)
	5.32	-0.0054(64)	-0.0020(14)	4.04(75)	-2.14(38)	0.95(93)
	5.34	0.000(6)	0.000(1)	2.99(53)	-1.51(26)	0.99(60)
	5.36	0.0031(55)	0.0038(13)	2.22(46)	-1.06(22)	0.89(54)
	5.40	0.0057(50)	-0.0010(12)	1.72(41)	-0.56(19)	1.08(47)

Table 4.3: Responses of the pseudoscalar meson to $\hat{\mu}_V$.

4.3 Responses of the pseudoscalar meson to the isovector chemical potential

Results for the isovector chemical potential are summarized in Table 4.3. In the presence of the isovector chemical potential, π^+ and π^- may have different masses. Here we consider the π^+ ($u\bar{d}$) meson as shown in Eq. (2.1.5). In contrast to the case of the isoscalar chemical potential, the second order response of the mass is significantly large in the low temperature phase, and decreases in magnitude above T_c. The difference between the isoscalar and isovector chemical potentials is illustrated in right figure of Fig. 4.16. The response of $\hat{\gamma}$ also shows different behaviors in the confined and deconfined phases, illustrated in Fig. 4.18.

These features are manifest even for a small quark mass parameter. Note that the isovector potential explicitly breaks the u-d symmetry, even if the two quarks have equal masses. The phase structure in the ($T, |\mu_V|$) plane has been studied by Son and Stephanov [32]. The original $SU(2)_{L+R}$ symmetry at non-zero quark mass and zero chemical potential is broken down to $U(1)_{L+R}$. At zero T and for $|\mu_V|$ larger than the mass of the pseudoscalar, the system is in a different phase than at $\mu_V = 0$. The ground state is a pion condensate and there is one massless Goldstone boson associated with the spontaneous breaking of the $U(1)_{L+R}$ symmetry. For $|\mu_V| = m_{PS}$, the critical temperature

is $T = 0$. At sufficiently high temperature, the condensate melts and the symmetry is restored. Due to the presence of the phase boundary, we do not expect to be able to reach the condensed phase by Taylor expanding around $\mu_V = 0$. We can, however, hope to get some hints about the presence of the phase boundary while keeping $|\mu_V| < m_{PS}$. In this case, the system is in the same ground state as for zero chemical potential, there are no exact Goldstone modes and the three pions are massive.

An interesting point in this respect is that the second derivative of the mass is negative in the low temperature phase, in marked contrast with what happened for the isoscalar potential. The mass tends to decrease under the influence of the isovector chemical potential, reflecting the fact that for low temperature and chemical potential above the pion mass, a Goldstone mode appears [7, 32]. This is more clearly shown by an expansion as in Eq. (2.0.1). At $\beta = 5.26$ and $ma = 0.017$, the data suggest

$$\begin{aligned} \left.\frac{M(\mu_V)}{T}\right|_{\mu_V} &= (1.4024 \pm 0.0008) + (-0.0005 \pm 0.0010) \left(\frac{\mu_V}{T}\right) \\ &- (1.31 \pm 0.04) \left(\frac{\mu_V}{T}\right)^2 + O\left[\left(\frac{\mu_V}{T}\right)^3\right] \quad . \end{aligned} \tag{4.3.1}$$

The coefficient of the linear term is consistent with zero. Notice also in Table III that the lighter the quark mass, the stronger the response, a possible indication that for lighter pions the phase boundary is closer to the zero chemical potential axis, as suggested in [32].

In the high temperature phase, the dependence of the masses on μ_V decreases. Since the pseudoscalar meson becomes heavier, the phase boundary to the pion condensate phase is farther away from the $\mu_V = 0$ axis. The weaker responses may be understood from this point of view.

4.4 Results for the vector meson

As for the vector meson, correlators are calculable at $\beta = 5.26$ and $\beta = 5.34$ for $ma = 0.0250$. But the signal noise ratio is very bad. At present, the screening mass and the responses are extracted from a limited range of the data. In Table 4.4, we summarize screening masses of the vector meson. We find the error bars are larger than these for pseudoscalar meson masses and the masses are slightly changed between low temperature

$ma \setminus \beta$	5.26				5.34				
0.0125	1.287(54)				1.295(20)				
0.0170	1.287(54)				1.312(17)				
$ma \setminus \beta$	5.20	5.26	5.28	5.29	5.30	5.32	5.34	5.36	5.40
0.0250	1.450 (56)	1.320 (29)	1.365 (34)	1.383 (28)	1.51 (36)	1.299 (13)	1.352 (52)	1.311 (27)	1.387 (27)

Table 4.4: Preliminary results for vector meson masses.

and high temperature. The first order response to the isovector chemical potential is again small and consistent with zero (see Fig. 4.19).

Fig. 4.20 shows the vector meson correlator and the second order responses of the correlator to the isoscalar and isovector chemical potentials for $ma = 0.025$ and $\beta = 5.26$. As for the second order response, a positive response to the isoscalar chemical potential is indicated in low temperature, whereas it is negative to the isovector potential. In comparison with the responses of the pseudoscalar meson, for example $d^2\hat{M}/d\hat{\mu}_V^2$, the responses are weak.

Let us turn to the data in high temperature phase. In Fig. 4.21, we plot the vector meson correlator at $\beta = 5.34$, $ma = 0.025$, and the free quark correlator at $ma = 0.025$. Their responses are shown in Fig. 4.22. The correlator and its response show very different shapes from those of the pseudoscalar meson. Apparently, formulas based on the single meson pole dominance, Eq. (2.1.1)–Eq. (2.1.3) give very poor description to the data. Rather, a mesonic correlator composed of free quarks gives similar shapes for the correlator and responses as shown in Fig. 4.21 and Fig. 4.22. Thus, in contrast to the pseudoscalar meson, the data suggest deconfining of hadronic cluster in the vector channel. High statistical simulations shall be required to clarify the behavior.

4.5 Numerical results for responses of condensate

From Eq. (3.2.4) and Eq. (3.3.4), the first order response of $\langle \bar{\psi}\psi \rangle$ to the isoscalar and isovector chemical potentials in lattice QCD are zero. To investigate the behavior of a system at small chemical potential, we must explore the second response of $\langle \bar{\psi}\psi \rangle$ to

	5.20	5.26	5.28	5.29	5.30	5.32	5.34	5.36	5.40
$\langle\bar{\psi}\psi\rangle$	0.4576 (3)	0.3931 (5)	0.3423 (1)	0.2682 (2)	0.1758 (2)	0.1325 (8)	0.1126 (5)	0.1013 (6)	0.0875 (4)
$\frac{\partial^2\langle\bar{\psi}\psi\rangle}{\partial\mu_S^2}$	-0.3 (20)	-1.1 (19)	-3.9 (29)	-12.5 (20)	-4.1 (15)	-1.90 (55)	-1.03 (31)	-0.85 (37)	-0.56 (26)
$\frac{\partial^2\langle\bar{\psi}\psi\rangle}{\partial\mu_V^2}$	-0.38 (70)	-1.09 (83)	-3.7 (15)	-11.3 (15)	-3.8 (11)	-1.73 (38)	-1.01 (23)	-0.83 (28)	-0.56 (21)

Table 4.5: $\langle\bar{\psi}\psi\rangle$, $\frac{\partial^2\langle\bar{\psi}\psi\rangle}{\partial\mu_S^2}$ and $\frac{\partial^2\langle\bar{\psi}\psi\rangle}{\partial\mu_V^2}$ for $ma = 0.025$.

the isoscalar and isovector chemical potentials. We summarize our simulation results for responses of chiral condensate in Table 4.5. In Fig. 4.23, we plot the responses of $\langle\bar{\psi}\psi\rangle$ to the isoscalar and isovector chemical potentials as a function of $\frac{T}{T_C}$. In the chiral broken symmetry phase, the second order response of $\langle\bar{\psi}\psi\rangle$ is negative and small. In this case $\langle\bar{\psi}\psi\rangle$ decreases as μ is increased. In the chiral symmetry restoration phase, the second order response of $\langle\bar{\psi}\psi\rangle$ are also negative. The behavior of $\langle\bar{\psi}\psi\rangle$ decreases faster than that in the chiral broken symmetry phase. In addition, in chiral symmetry restoration phases $\langle\bar{\psi}\psi\rangle$ is zero in the continuum limit, and the responses of $\langle\bar{\psi}\psi\rangle$ are zero. Our simulation results are not in contradiction with those in the continuum limit. This is more clearly shown by expansion as in Eq. (3.0.1).

Near β_C, for instance, $\beta = 5.29$,

$$\begin{aligned}\left.\frac{\langle\bar{\psi}\psi\rangle(\mu_S)}{T^3}\right|_{\mu_S} &= (17.16 \pm 0.11) - (25.0 \pm 4.1)\left(\frac{\mu_S}{T}\right)^2 + O\left[\left(\frac{\mu_S}{T}\right)^3\right] \\ \left.\frac{\langle\bar{\psi}\psi\rangle(\mu_V)}{T^3}\right|_{\mu_V} &= (17.16 \pm 0.11) - (22.6 \pm 3.0)\left(\frac{\mu_V}{T}\right)^2 + O\left[\left(\frac{\mu_V}{T}\right)^3\right]. \quad (4.5.1)\end{aligned}$$

there are large responses. The contribution of chemical potential makes β_C to drop off from $\mu = 0$.

In the chiral symmetry restoration phases,

$$\begin{aligned}\left.\frac{\langle\bar{\psi}\psi\rangle(\mu_S)}{T^3}\right|_{\mu_S} &= (6.486 \pm 0.039) - (1.70 \pm 0.75)\left(\frac{\mu_S}{T}\right)^2 + O\left[\left(\frac{\mu_S}{T}\right)^3\right] \\ \left.\frac{\langle\bar{\psi}\psi\rangle(\mu_V)}{T^3}\right|_{\mu_V} &= (6.486 \pm 0.039) - (1.65 \pm 0.56)\left(\frac{\mu_V}{T}\right)^2 + O\left[\left(\frac{\mu_V}{T}\right)^3\right], \quad (4.5.2)\end{aligned}$$

at $\beta = 5.36$, and

$$\begin{aligned}\left.\frac{\langle\bar{\psi}\psi\rangle(\mu_S)}{T^3}\right|_{\mu_S} &= (5.598 \pm 0.025) - (1.12 \pm 0.53)\left(\frac{\mu_S}{T}\right)^2 + O\left[\left(\frac{\mu_S}{T}\right)^3\right] \\ \left.\frac{\langle\bar{\psi}\psi\rangle(\mu_V)}{T^3}\right|_{\mu_V} &= (5.598 \pm 0.025) - (1.12 \pm 0.43)\left(\frac{\mu_V}{T}\right)^2 + O\left[\left(\frac{\mu_V}{T}\right)^3\right], \quad (4.5.3)\end{aligned}$$

at $\beta = 5.40$. We find the response for the isoscalar chemical potential is similar to that for the isovector channel.

Using Eq. (3.0.1), we also plot our results for the small finite chemical potential. In the Fig. 4.24, we include $\langle\bar{\psi}\psi\rangle$ for $\hat{\mu} = 0.10$ and $\hat{\mu} = 0.15$. We find the critical temperature tends to decrease under the influence of $\hat{\mu}_{S,V}$. Thus, in the low temperature phase, turning on the chemical potential brings the system closer to the phase transition where chiral symmetry is restored, and decreases the chiral condensate. At high temperature, because chiral symmetry is restored, responses of the chiral condensate to the isoscalar and isovector chemical potential are small.

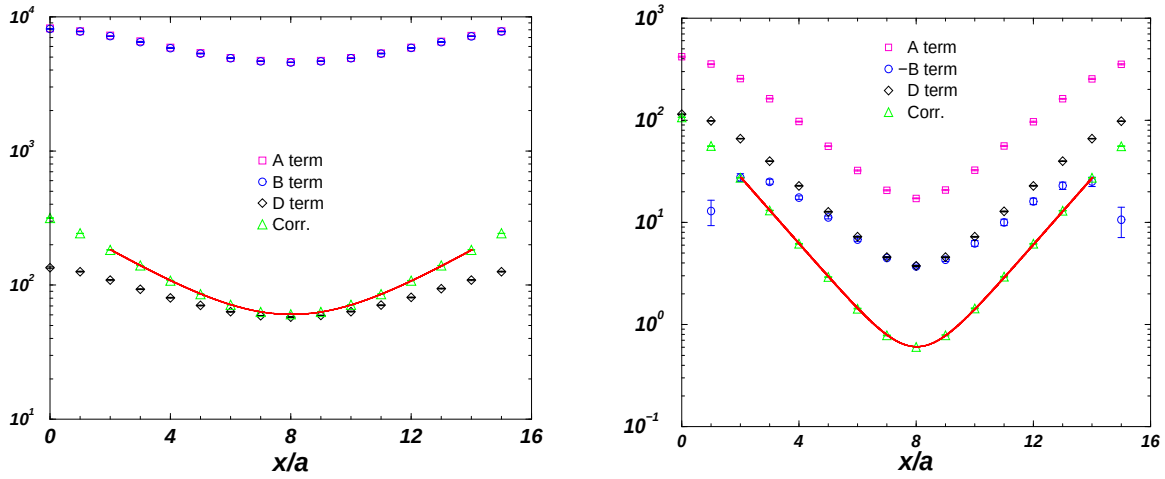

Figure 4.3: Correlator and some quantities of the pseudoscalar meson at $\beta = 5.26$ (left figure), 5.34 (right figure) and $ma = 0.0125$. The curve is fitted by the single pole formula (2.1.1).

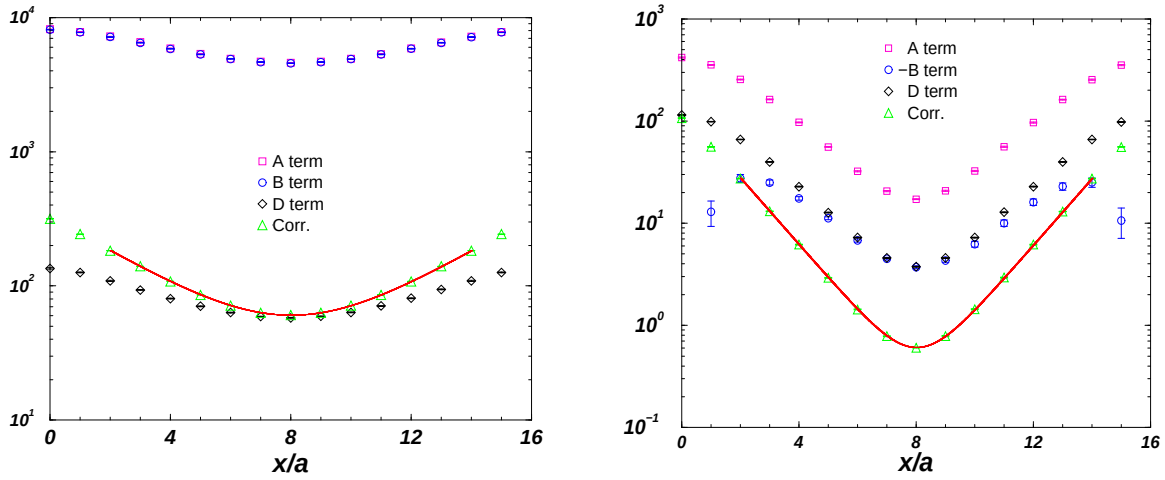

Figure 4.4: Correlator and some quantities of the pseudoscalar meson at $\beta = 5.26$ (left figure), 5.34 (right figure) and $ma = 0.0125$. The curve is fitted by the single pole formula (2.1.1).

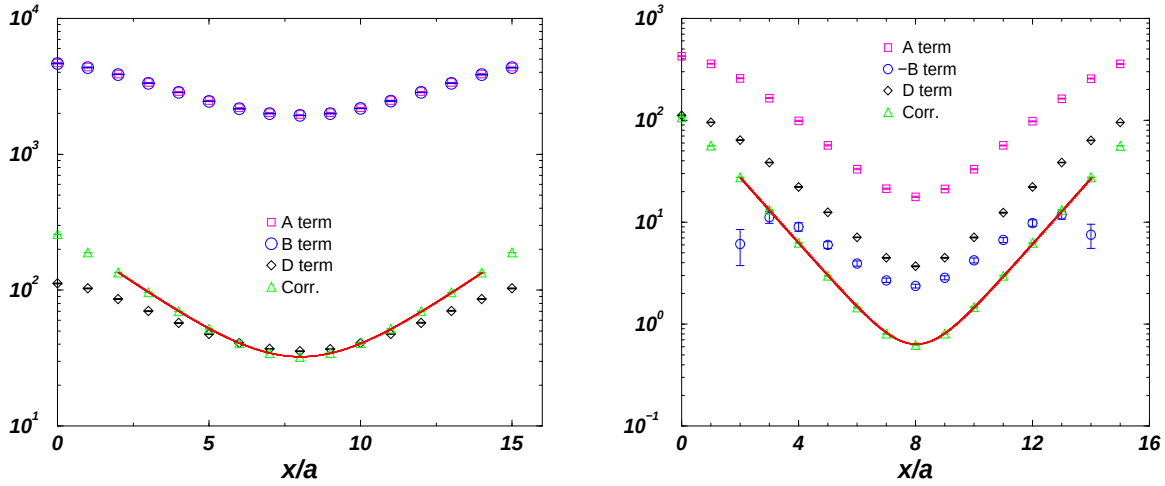

Figure 4.5: Correlator and some quantities of the pseudoscalar meson at $\beta = 5.26$ (left figure), 5.34 (right figure) and $ma = 0.0170$. The curve is fitted by the single pole formula (2.1.1).

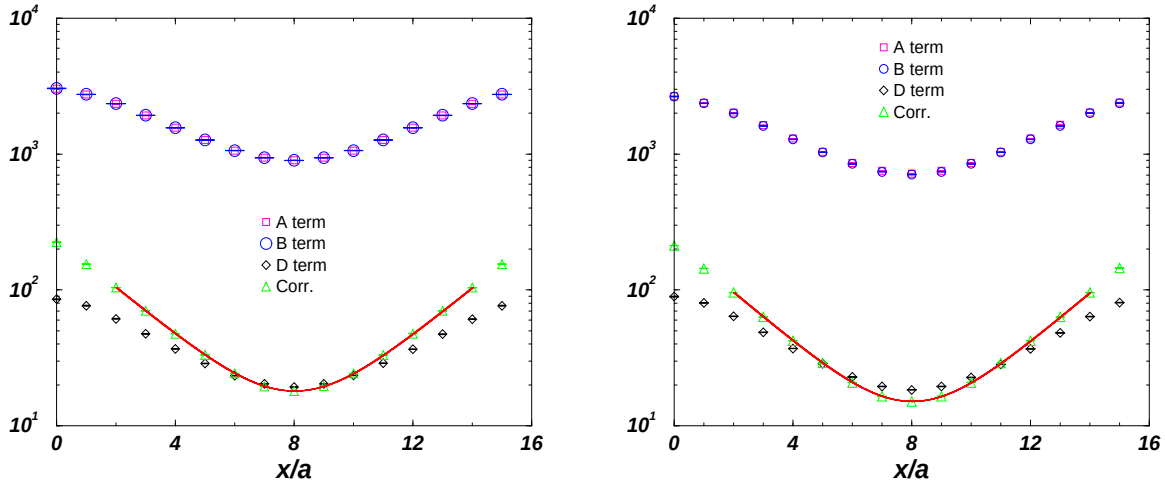

Figure 4.6: Correlator and some quantities of the pseudoscalar meson at $\beta = 5.20$ (left figure), 5.26 (right figure) and $ma = 0.0250$. The curve is fitted by the single pole formula (2.1.1).

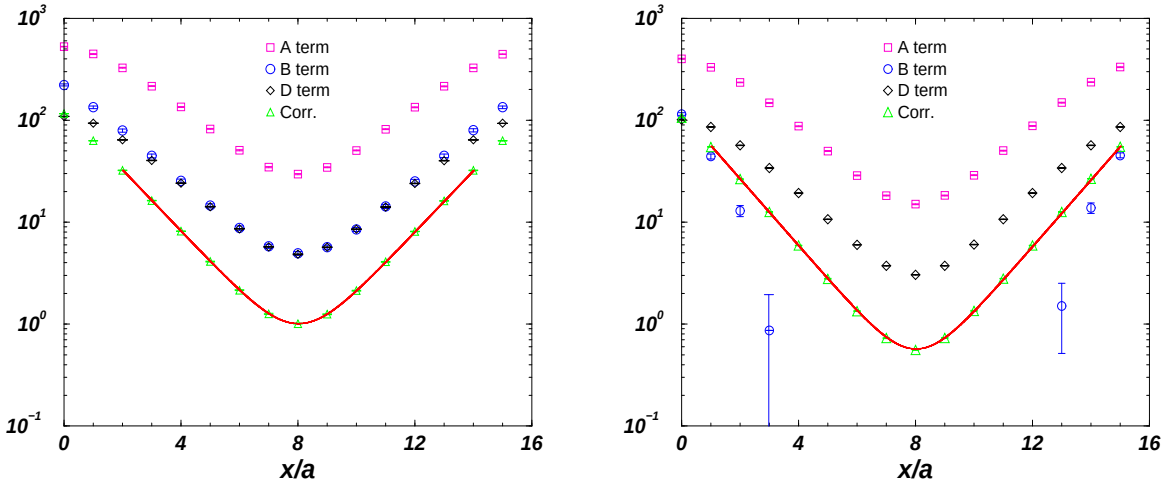

Figure 4.7: Correlator and some quantities of the pseudoscalar meson at $\beta = 5.32$ (left figure), 5.34 (right figure) and $ma = 0.0250$. The curve is fitted by the single pole formula (2.1.1).

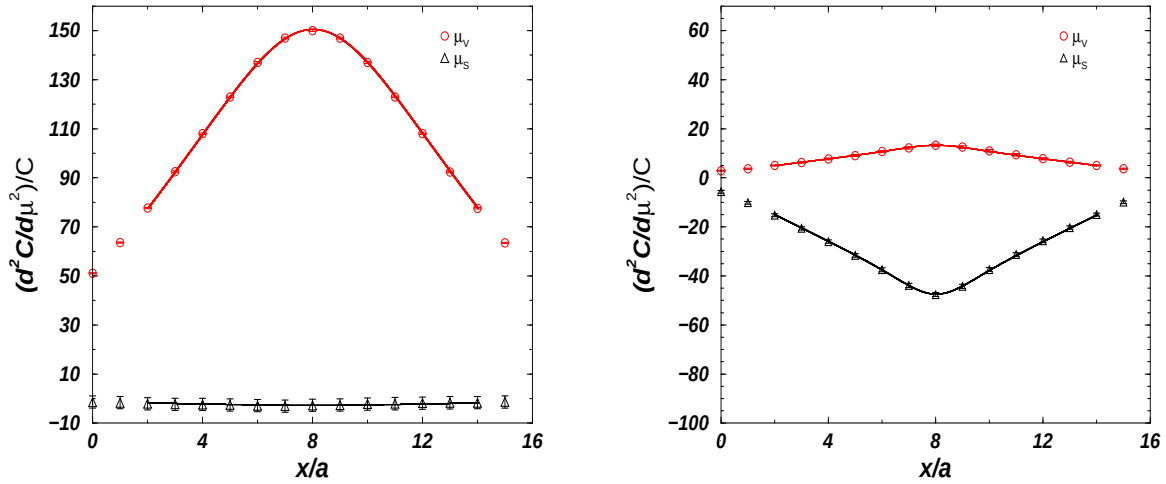

Figure 4.8: The second order response of the pseudoscalar meson correlator at $\beta = 5.26$ (left figure), and the same quark mass parameter $ma = 0.0125$ but $\beta = 5.34$ (right figure). The curves are fittings by the formula (2.1.3).

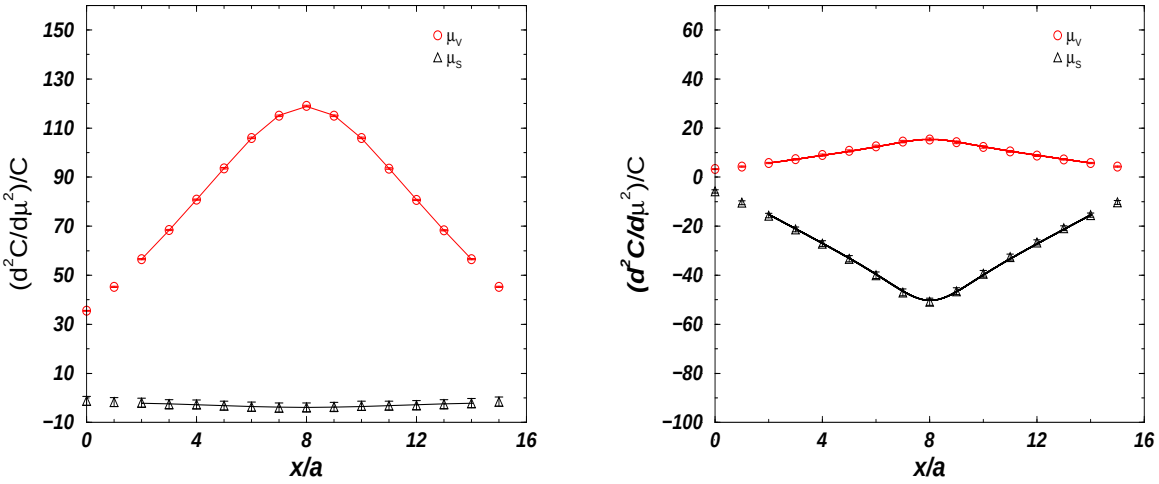

Figure 4.9: The second order response of the pseudoscalar meson correlator at $\beta = 5.26$ (left figure), and the same quark mass parameter $ma = 0.0170$ but $\beta = 5.34$ (right figure). The curves are fittings by the formula (2.1.3).

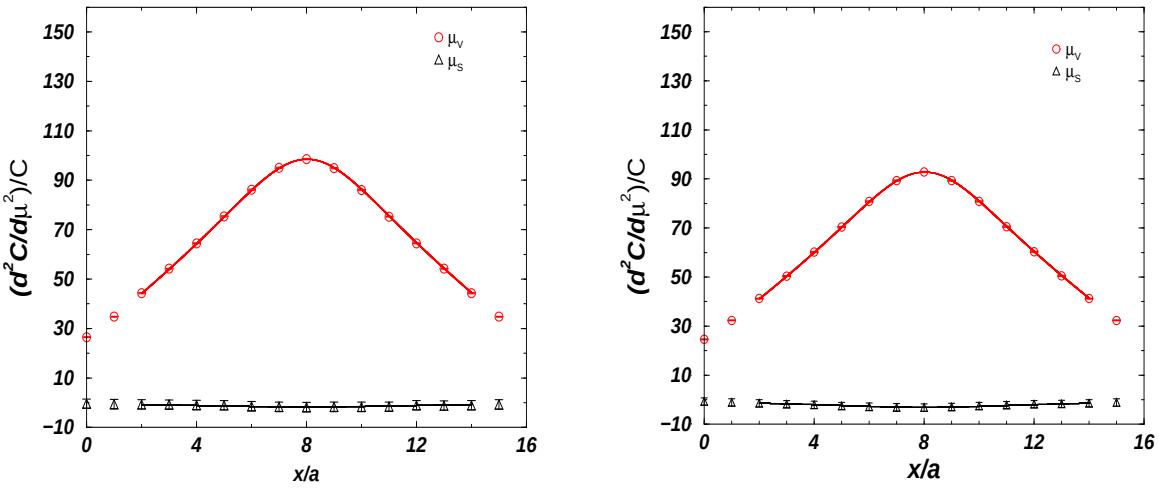

Figure 4.10: The second order response of the pseudoscalar meson correlator at $\beta = 5.20$ (left figure), and the same quark mass parameter $ma = 0.0250$ but $\beta = 5.26$ (right figure). The curves are fittings by the formula (2.1.3).

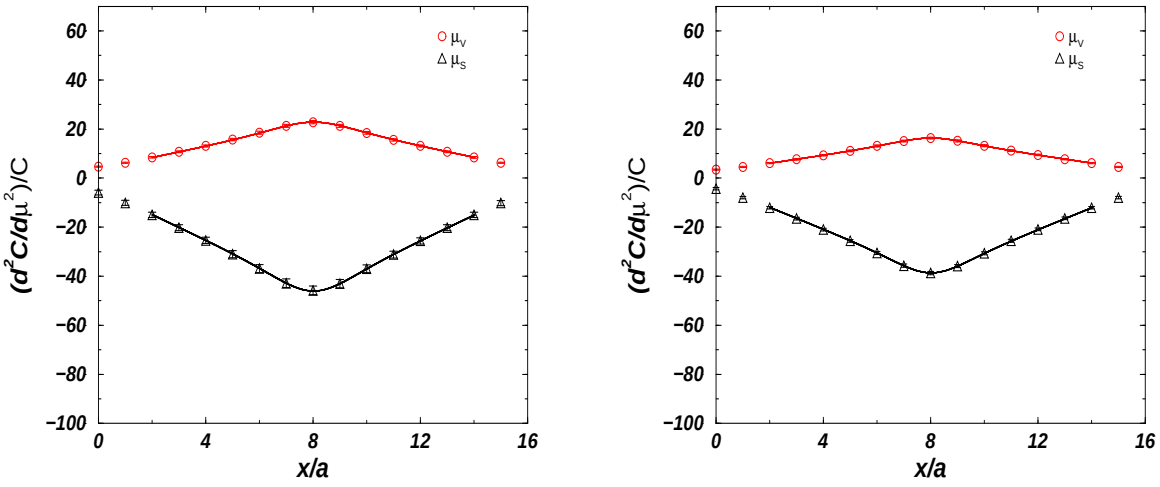

Figure 4.11: The second order response of the pseudoscalar meson correlator at $\beta = 5.32$ (left figure), and the same quark mass parameter $ma = 0.0250$ but $\beta = 5.34$ (right figure). The curves are fittings by the formula (2.1.3).

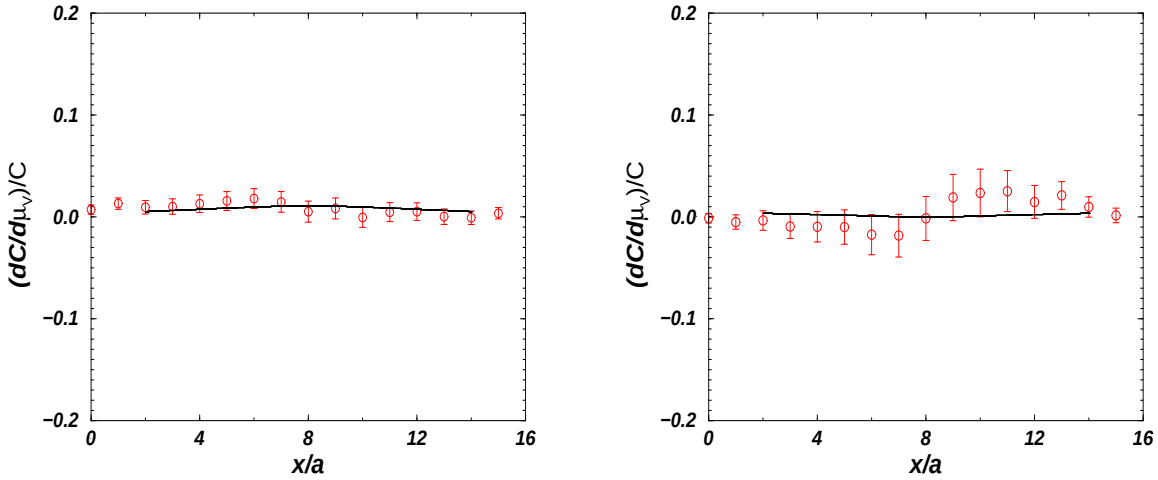

Figure 4.12: The first order response of the pseudoscalar meson correlator at $\beta = 5.26$ (left figure) and $\beta = 5.34$ (right figure). Quark mass parameter is $ma = 0.0125$. Line are fittings by the formula (2.1.2).

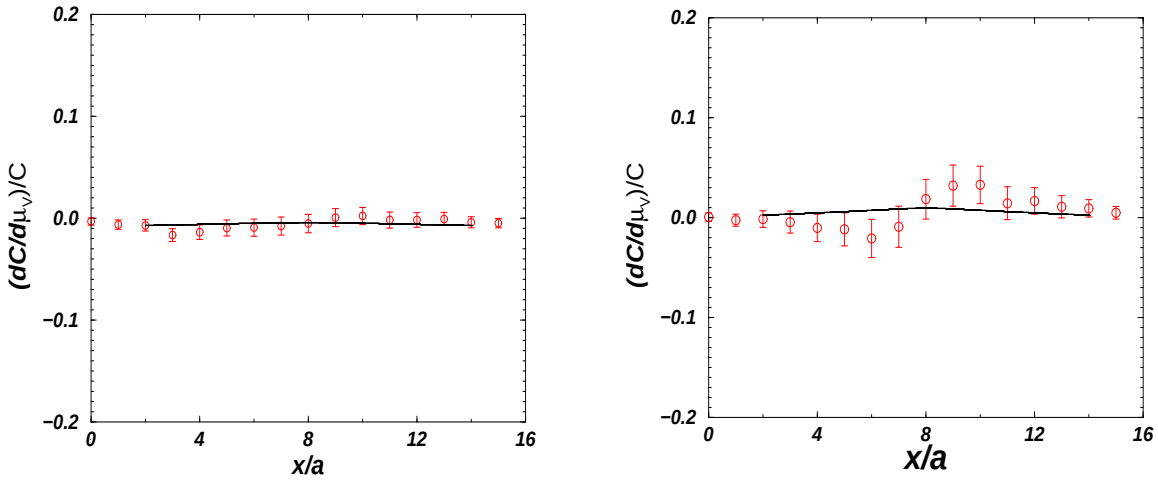

Figure 4.13: The first order response of the pseudoscalar meson correlator at $\beta = 5.26$ (left figure) and $\beta = 5.34$ (right figure). Quark mass parameter is $ma = 0.0170$. Line are fittings by the formula (2.1.2).

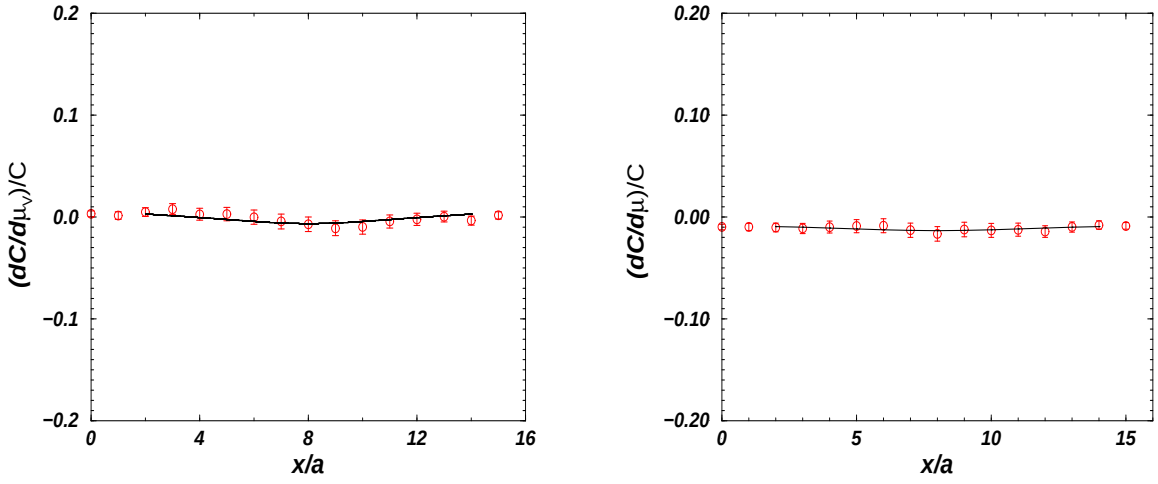

Figure 4.14: The first order response of the pseudoscalar meson correlator at $\beta = 5.20$ (left figure) and $\beta = 5.26$ (right figure). Quark mass parameter is $ma = 0.0250$. Line are fittings by the formula (2.1.2).

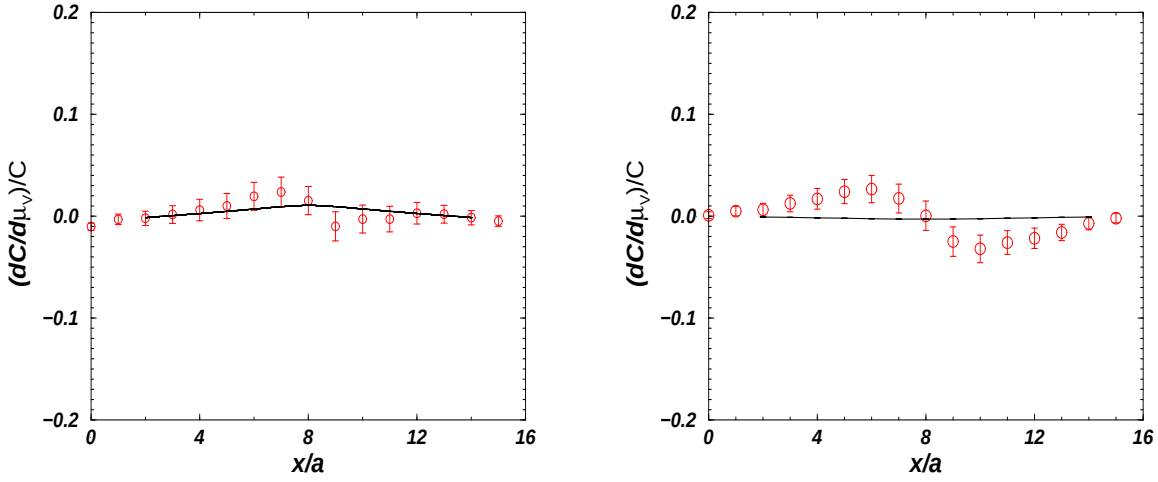

Figure 4.15: The first order response of the pseudoscalar meson correlator at $\beta = 5.32$ (left figure) and $\beta = 5.34$ (right figure). Quark mass parameter is $ma = 0.0250$. Line are fittings by the formula (2.1.2).

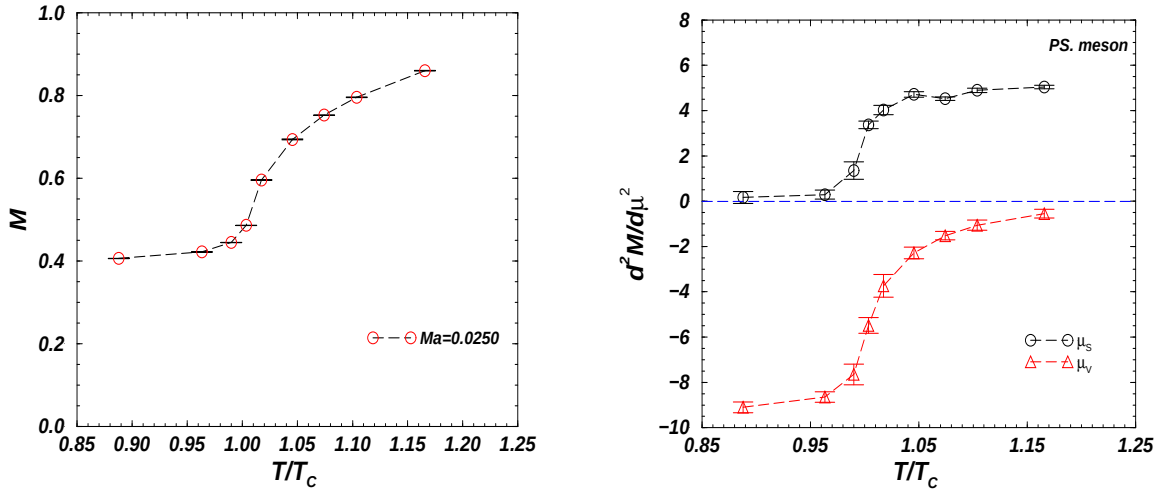

Figure 4.16: Screening mass of the pseudoscalar meson (left figure) and the second order response of its square (right figure) at $ma = 0.025$ in a^{-1} unit.

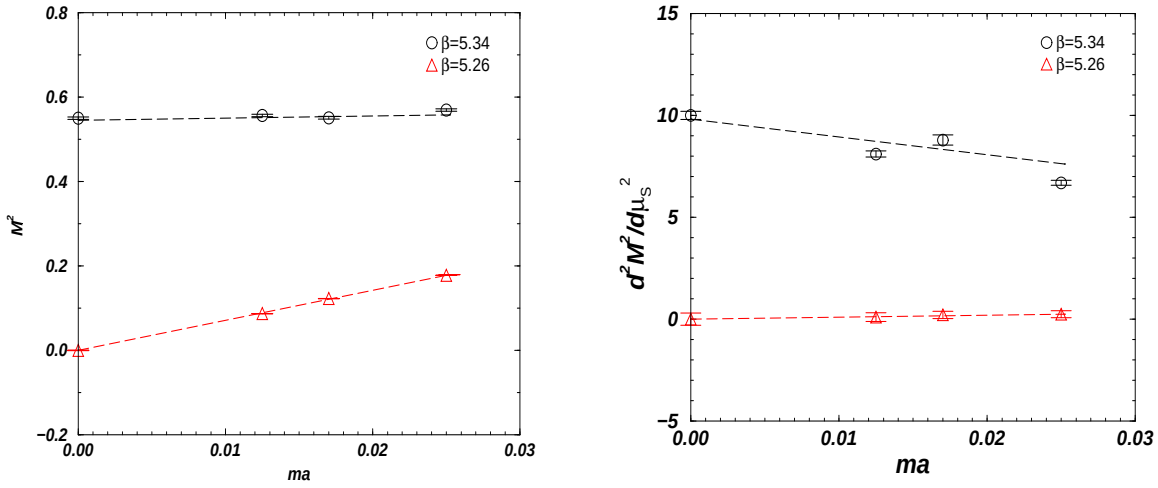

Figure 4.17: $\hat{M}^2$ (left figure) and $d^2\hat{M}^2/d\hat{\mu}_S^2$ (right figure) of the pseudoscalar meson versus ma. β are 5.26 (triangles) and 5.34 (circles). The symbols plotted at $ma = 0.0$ are the values extrapolated to $m = 0.0$.

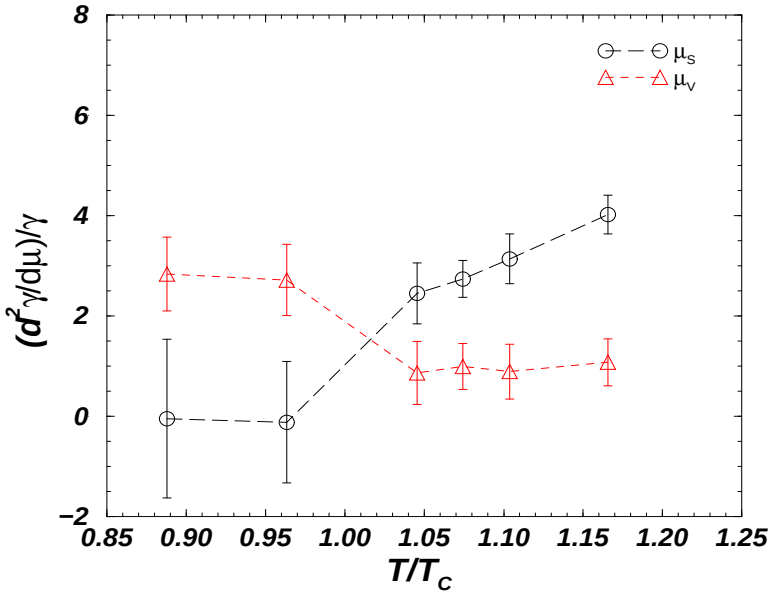

Figure 4.18: $\hat{\gamma}^{-1}d^2\hat{\gamma}/d\hat{\mu}_S^2$, $\hat{\gamma}^{-1}d^2\hat{\gamma}/d\hat{\mu}_V^2$ of the pseudoscalar meson at $ma = 0.025$.

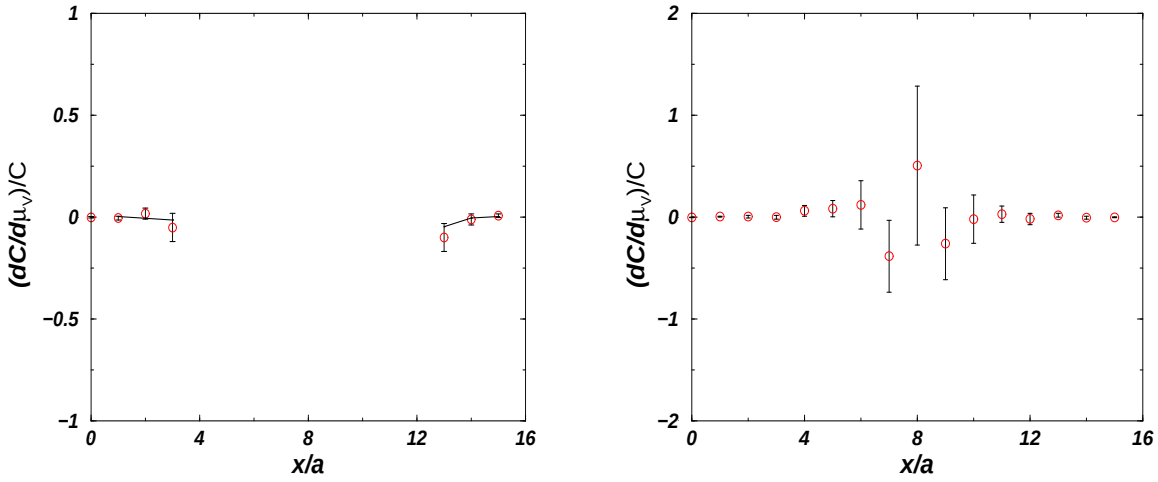

Figure 4.19: The first response of vector meson correlator at $\beta = 5.26$ (left figure) and $\beta = 5.34$(right figure) for $ma = 0.025$.

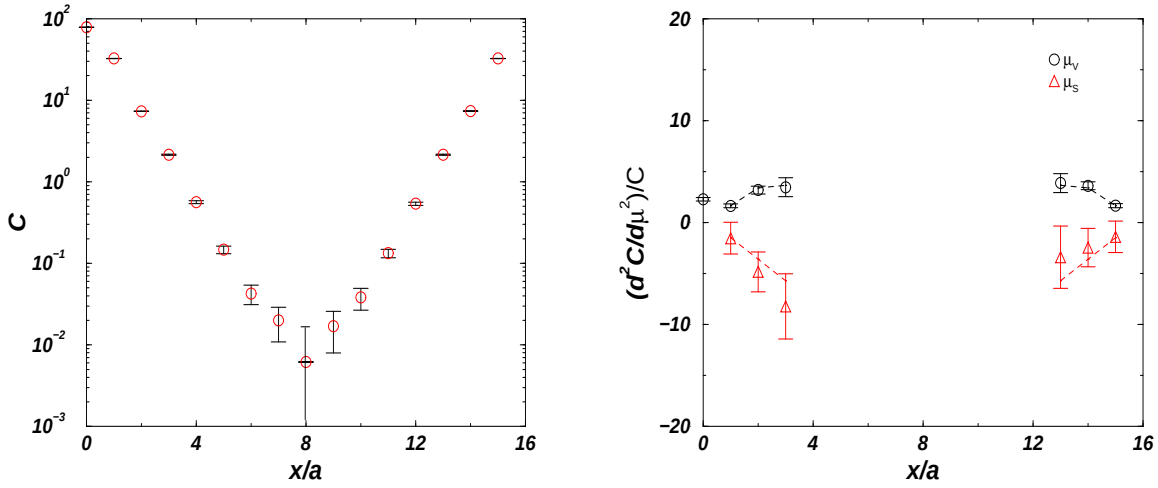

Figure 4.20: Vector meson correlator at $\beta = 5.26$ and $ma = 0.025$ (left figure), and the second order response of the correlator (right figure).

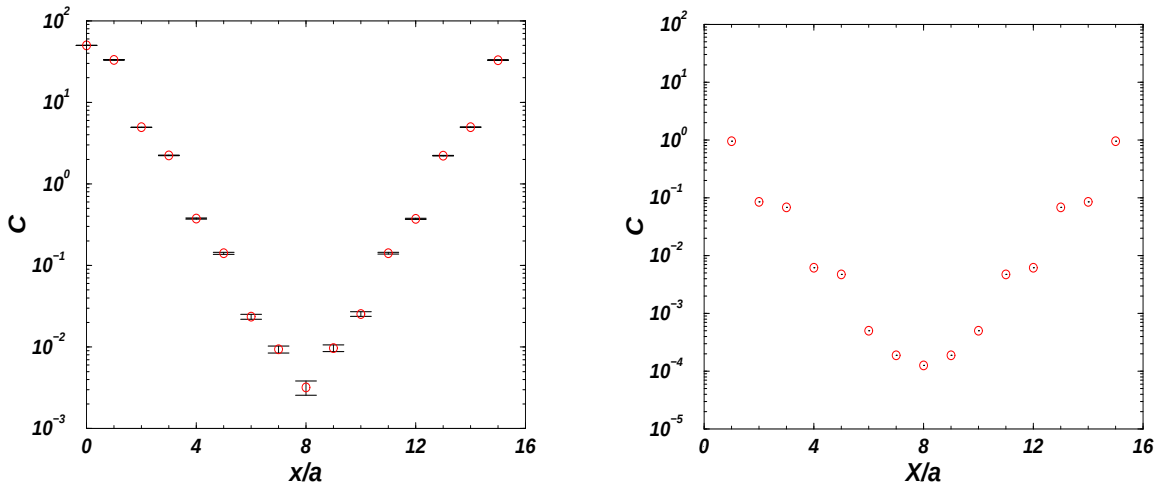

Figure 4.21: Vector meson correlator at $\beta = 5.34$ and $ma = 0.025$ (left figure), and free quark correlator (right figure) at $ma = 0.025$.

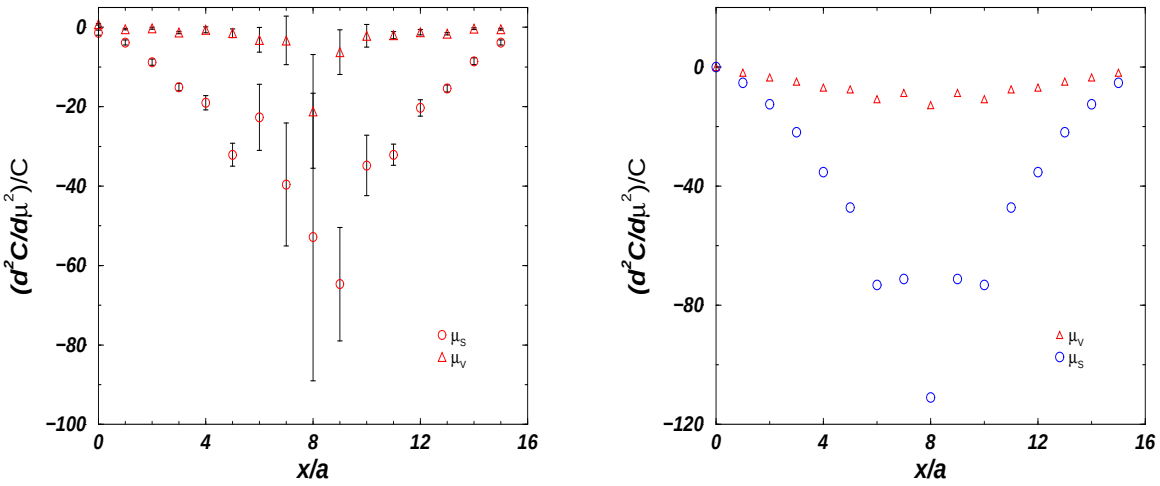

Figure 4.22: The second order response of vector meson at $\beta = 5.34$ and $ma = 0.025$ (left figure), and free quark response (right figure) at $ma = 0.025$.

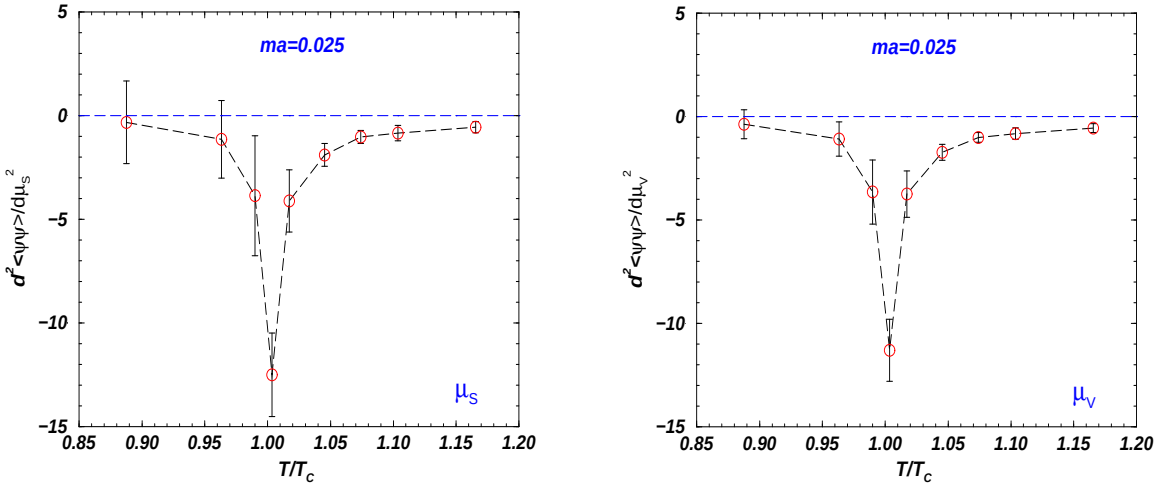

Figure 4.23: $\frac{\partial^2\langle\bar{\psi}\psi\rangle}{\partial\hat{\mu}_S^2}$ (left figure) and $\frac{\partial^2\langle\bar{\psi}\psi\rangle}{\partial\hat{\mu}_V^2}$ (right figure) as a function of $\frac{T}{T_c}$ at $ma = 0.025$.

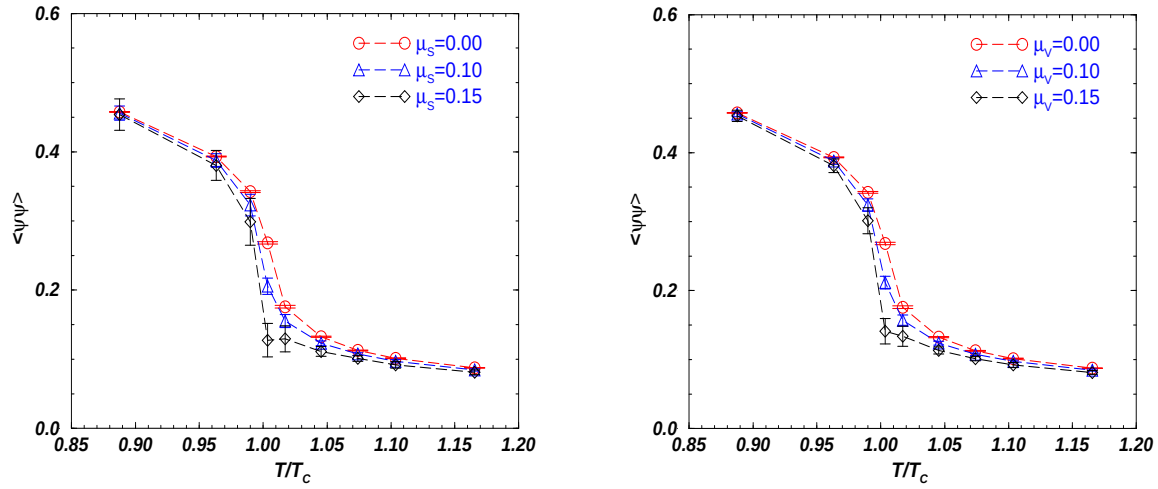

Figure 4.24: Behavior of $\langle\bar{\psi}\psi\rangle$ at finite isoscalar chemical potential (left figure) and the isovector chemical potential (right figure).

Conclusions and Perspectives

In this work, we have developed a framework for the second order response to the chemical potential and shown the first results of the first and second responses of pseudoscalar and vector meson masses. As shown in the previous sections, the second order responses are sizable and reveal several characteristic features. For the pseudoscalar meson, the behavior of the responses seems to have close contact to the chiral restoration. It is notable that the single hadron pole gives a good description for the response as well as for the correlator at $\beta = 5.34$ ($T/T_c \approx 1.1$) in the pseudoscalar channel. On the other hand, the vector meson is not well fitted by the single pole equation and seems to be deconfined there.

Since the present study is the first trial, our simulations have been performed on a rather small lattice. However, differences $N_t = 4$ and $N_t = 6$ lattices have been reported [36]. Thus, further investigations on larger lattices are indispensable. A study of the chemical potential response of the nucleon is also interesting. An exploratory study is in progress.

Appendix A

A.1 Non-zero fermion number density

Up to now thermodynamics of hadronic matter was discussed at high temperature and vanishing net fermion number density (In the low energy, net baryon number density is one third of the fermion number density). At non-vanishing fermion number density, using the grand canonical partition function $Z(T,\mu_q) \equiv \mathrm{Tr}\{\exp\left[-\frac{1}{T}(H-\mu_q N_q)\right]\}$, with the Hamiltonian H and fermion number operator N_q, n_q can be calculated from

$$n_q = \frac{T}{V}\frac{\partial \ln Z}{\partial \mu_q} = \frac{a^{-3}}{L_s^3 L_t}\frac{\partial \ln Z}{\partial \mu_q} \tag{A.1.1}$$

where an isotropic lattice spacing (a) is assumed.

An introduction of the quark chemical potential μ_q in the QCD lattice action has to satisfy the trivial requirement that for free quarks (without color gauge interaction) the well-known results for the ideal relativistic Fermi gas have to be reproduced in the continuum limit. The quark matrix D for Wilson quarks with non-zero chemical potential on an isotropic lattice can be written as [37, 38, 39, 40]

$$\begin{aligned} D_{y,x} = \delta_{y,x} - K\sum_{n=1}^{3}\big[&\delta_{y,x+\hat{n}}(r+\gamma_n)U_{x,n} \\ &+\delta_{x,y+\hat{n}}(r-\gamma_n)U^{\dagger}_{x,n}\big] \\ -KF(a\mu_q)&\delta_{y,x+\hat{4}}(r+\gamma_4)U_{x,4} \\ -KG(a\mu_q)&\delta_{y+\hat{4},x}(r-\gamma_4)U^{\dagger}_{x,4}. \end{aligned} \tag{A.1.2}$$

Here F and G are, for the moment, arbitrary functions of chemical potential in lattice

units ($a\mu_q$), to be determined later. Similarly, for staggered quarks,

$$D_{y,x} = am\delta_{y,x} + \frac{1}{2}\sum_{n=1}^{3}\eta_{x,n}\left[\delta_{y+\hat{n},x}U^{\dagger}_{y,n} - \delta_{y,x+\hat{n}}U_{x,n}\right] + \frac{1}{2}\eta_{x,4}[G(a\mu_q)\delta_{y+\hat{4},x}U^{\dagger}_{y,4} - F(a\mu_q)\delta_{y,x+\hat{4}}U_{x,4}]. \quad \text{(A.1.3)}$$

In order to constrain the functions $F(a\mu_q)$ and $G(a\mu_q)$, let us consider the free energy density f [41] in the absence of gauge interaction ($U_{x,\mu} = 1$)

$$f = -\frac{T}{V}\ln Z = -T^4\frac{L_t^3}{L_s^3}\ln Z, \quad \text{(A.1.4)}$$

where $T^{-1} = a_t L_t$, $V = (a_s L_s)^3$, and $a_t = a_s$. Performing the Grassmannian path integral, action can be defined

$$S_f = \ln\det(D). \quad \text{(A.1.5)}$$

One obtains

$$fT^{-4} = -\frac{L_t^3}{L_s^3}\ln\det(D) = -\frac{L_t^3}{L_s^3}\ln\det(\tilde{D}). \quad \text{(A.1.6)}$$

Here, in the second step a unitary transformation into momentum space was performed, which is defined by

$$\tilde{D}_{l,k} \equiv \frac{1}{L_s^3 L_t}\sum_{x,y} e^{\mathrm{i}y\cdot l + \mathrm{i}x\cdot k} D_{y,x}. \quad \text{(A.1.7)}$$

Using the Wilson quark matrix, Eq. (A.1.6) gives

$$fT^{-4} = -\frac{L_t^3}{L_s^3}\ln\det{}_{sc}\left\{1 - K\left[\sum_{n=1}^{3}\{2r\cos(k_n) - 2\mathrm{i}\gamma_n\sin(k_n)\} + 2rR\cos(k_4 + \mathrm{i}\theta) - 2\mathrm{i}R\gamma_4\sin(k_4 + \mathrm{i}\theta)\right]\right\}, \quad \text{(A.1.8)}$$

where R and θ are defined by

$$R \equiv (FG)^{\frac{1}{2}}, \qquad \tanh(\theta) = \frac{F-G}{F+G}$$
$$R\,\cosh(\theta) = \frac{1}{2}(F+G), \qquad R\,\sinh(\theta) = \frac{1}{2}(F-G). \quad \text{(A.1.9)}$$

Eq. (A.1.8) still contains the vacuum contribution, which can be removed by subtracting fT^4 at $\mu_q = 0$. Calculating the determinant in spinor-color indices $\det_{sc}$ gives

$$[f(T,\mu_q) - f(T,0)]T^{-4} =$$

$$-L_t^4 \frac{6}{L_s^3 L_t} \sum_k \left\{ \ln \left[\left(1 - 2rK \sum_{n=1}^{3} \cos(k_n) - 2rKR\cos(k_4 + \mathrm{i}\theta) \right)^2 \right.\right.$$
$$\left. + 4K^2 \sum_{n=1}^{3} \sin^2(k_n) + 4K^2 R^2 \sin^2(k_4 + \mathrm{i}\theta) \right]$$
$$\left. - \ln \left[\left(1 - 2rK \sum_{\mu=1}^{4} \cos(k_\mu) \right)^2 + 4K^2 \sum_{\mu=1}^{4} \sin^2(k_\mu) \right] \right\}. \qquad \text{(A.1.10)}$$

In the continuum limit $a \longrightarrow 0$ the momentum is $k_\mu = a p_\mu$, and in the limit L_s, $L_t \longrightarrow \infty$ the momentum sums become integrals by

$$\int_k \equiv \frac{1}{\Omega} \sum_k \Longrightarrow \frac{1}{(2\pi)^4} \int_0^{2\pi} d^4k = \frac{1}{(2\pi)^4} \int_{-\pi}^{\pi} d^4k,$$

where Ω is Fourier transformation factor. It turns out that the correct continuum limit is obtained only if

$$R \equiv 1, \qquad \theta(a\mu_q) = a\mu_q + O(a\mu_q)^2. \qquad \text{(A.1.11)}$$

Otherwise, at the critical value of the hopping parameter, the free energy density and other thermodynamic quantities diverge. This means that the simplest choice [37, 38]

$$F(a\mu_q) = \frac{1}{G(a\mu_q)} = e^{a\mu_q} \qquad \text{(A.1.12)}$$

is essentially unique at least near the continuum limit. In this case Eq. (A.1.10) gives

$$f(T, \mu_q) - f(T, 0) \longrightarrow -\frac{6}{(2\pi)^4} \int_{-\infty}^{\infty} d^4p \, \ln \frac{m^2 + \sum_{n=1}^{3} p_n^2 + (p_4 + \mathrm{i}\mu_q)^2}{m^2 + p^2}. \qquad \text{(A.1.13)}$$

It can also be shown that in the continuum limit the choice of Eq. (A.1.12) gives the correct energy and number density of an ideal relativistic Fermi gas [37, 39].

The numerical simulation of QCD at non-zero quark chemical potential $\mu_q \neq 0$ is difficult. For $\mu_q = 0$ we have

$$S_q = \sum_{x,y} \left(\bar{\psi}_y D[U]_{y,x} \psi_x \right), \qquad \text{(A.1.14)}$$

and the quark matrix satisfies the relation

$$D_{y,x} = \gamma_5 D^\dagger_{x,y} \gamma_5, \qquad \text{(A.1.15)}$$

where $D^{\dagger}_{x,y}$ denotes the adjoint with respect to the Dirac spinor and color indices. Therefore the quark determinant is real, because

$$\det D = \det D^{\dagger} = (\ det\ D\ )^{*}. \tag{A.1.16}$$

However, the relation Eq. (A.1.16) does not hold at $\mu_q \neq 0$. The quark determinant is complex, therefore the effective gauge action S_{eff} and the Boltzmann factor $e^{-S_{eff}}$ also become complex. This means that $e^{-S_{eff}}$ can not be used for the transition probability in an updating process. In principle one can define the transition probability by the absolute value of the quark determinant:

$$\det D \equiv e^{i\varphi D}|\det D| = e^{i\varphi D}[\ \det DD^{\dagger}\ ]^{\frac{1}{2}}. \tag{A.1.17}$$

$$S_{eff}[U] \equiv S_G[U] - \frac{1}{2}\ln\ [\det(DD^{\dagger})] = S_G[U] - \frac{1}{2}\mathrm{Tr}\ [\det(DD^{\dagger})], \tag{A.1.18}$$

and include its phase in the measurement. For instance, for a pure gluonic quantity $A[U]$, one can use

$$\langle A[U]\rangle = \frac{\langle A[U]e^{\mathrm{i}\varphi D}\rangle_{S_{eff}}}{\langle e^{\mathrm{i}\varphi D}\rangle_{S_{eff}}}. \tag{A.1.19}$$

The problem with this mathematically correct representation is that, in practice, it usually does not work. Namely, $e^{i\varphi D}$ has a very strong fluctuation on the typical configurations in an updating process, which is generated by S_{eff} in Eq. (A.1.18). Such an updating process produces 'wrong' configurations with the wrong values of the measurable quantities. These contributions have to canceled by a strongly fluctuating phase. Therefore Eq. (A.1.19) can only be used on small lattices and for small chemical potentials [42].

Appendix B

B.1 Formulas for the isoscalar chemical potential response

The simulation for studying responses of hadrons is carried out at zero chemical potential with Eq. (2.1.14). In this paper we study two cases of chemical potential, i.e., the isoscalar and isovector type chemical potentials.

B.1.1 Response for hadron masses

Using Eq. (2.2.1), the quark and meson propagators have the following relations

$$g(\hat{\mu}_d)_{0;n} = \gamma_5 g^\dagger(-\hat{\mu}_d)_{n;0}\gamma_5 \quad , \tag{B.1.1}$$

and with the help of Eq.(B.1.1) G is given by

$$G = \mathrm{Tr}\left[g(\hat{\mu}_S)_{n:0}\Gamma\gamma_5 g(-\hat{\mu}_S)^\dagger_{n:0}\gamma_5\Gamma^\dagger\right] \quad , \tag{B.1.2}$$

where Tr means the trace over spinor and color indices. Each propagator is expanded as

$$\begin{aligned} g(\hat{\mu}) &= g - \hat{\mu} g\dot{D}g + \frac{\hat{\mu}^2}{2}\left(2g\dot{D}g\dot{D}g - g\ddot{D}g\right) + O(\hat{\mu}^3) \quad , \\ g(-\hat{\mu}) &= g + \hat{\mu} g\dot{D}g + \frac{\hat{\mu}^2}{2}\left(2g\dot{D}g\dot{D}g - g\ddot{D}g\right) + O(\hat{\mu}^3) \quad , \end{aligned} \tag{B.1.3}$$

where g and D are the propagator and the fermion operator at zero chemical potential, respectively, and a relation

$$\dot{g} = -g\dot{D}g \tag{B.1.4}$$

is used.

The first derivative at $\hat{\mu}_S = 0$ is

$$\dot{G} = -2\mathrm{iImTr}\left[\left(g\dot{D}g\right)_{n:0}\Gamma\gamma_5 g^\dagger_{n:0}\gamma_5\Gamma^\dagger\right] \quad , \tag{B.1.5}$$

and the second derivative at $\hat{\mu}_S = 0$ is obtained as

$$\begin{aligned}\ddot{G} &= 4\mathrm{ReTr}\left[\left(g\dot{D}g\dot{D}g\right)_{n:0}\Gamma\gamma_5 g^\dagger_{n:0}\gamma_5\Gamma^\dagger\right] \\ &- 2\mathrm{ReTr}\left[\left(g\ddot{D}g\right)_{n:0}\Gamma\gamma_5 g^\dagger_{n;0}\gamma_5\Gamma^\dagger\right] - 2\mathrm{Tr}\left[\left(g\dot{D}g\right)_{n:0}\Gamma\gamma_5\left(g\dot{D}g\right)^\dagger_{n:0}\gamma_5\Gamma^\dagger\right] \quad .\end{aligned} \tag{B.1.6}$$

Let us turn to calculate the derivatives of Δ. Using the following equations ,

$$\begin{aligned}\frac{\partial}{\partial\hat{\mu}}\det(D) &= \mathrm{Tr}\left[\dot{D}g\right]\det D \quad , \\ \frac{\partial^2}{\partial\hat{\mu}^2}\det(D) &= \left\{\mathrm{Tr}\left[\ddot{D}g\right] - \mathrm{Tr}\left[\dot{D}g\dot{D}g\right] + \mathrm{Tr}\left[\dot{D}g\right]^2\right\}\det(D) \quad ,\end{aligned} \tag{B.1.7}$$

we have

$$\begin{aligned}\frac{\dot{\Delta}}{\Delta} &= 2\mathrm{Tr}\left[\dot{D}g\right] \quad , \\ \frac{\ddot{\Delta}}{\Delta} &= 2\mathrm{Tr}\left[\ddot{D}g\right] - 2\mathrm{Tr}\left[\dot{D}g\dot{D}g\right] + 4\mathrm{Tr}\left[\dot{D}g\right]^2 \quad .\end{aligned} \tag{B.1.8}$$

Combining Eqs.(2.1.14), (B.1.5), (B.1.7), (B.1.8) and (B.1.9), we have

$$\frac{\partial}{\partial\hat{\mu}} \quad \mathrm{Re}\langle H(n)H(0)^\dagger\rangle = 0 \quad , \tag{B.1.9}$$

and

$$\begin{aligned}\frac{\partial^2}{\partial\hat{\mu}^2} \quad \mathrm{Re} \quad &\left\langle H(n)H(0)^\dagger\right\rangle = 4\mathrm{Re}\left\langle\mathrm{Tr}\left[\left(g\dot{D}g\dot{D}g\right)_{n:0}\Gamma\gamma_5 g^\dagger_{n:0}\gamma_5\Gamma^\dagger\right]\right\rangle \\ &- 2\mathrm{Re}\left\langle\mathrm{Tr}\left[\left(g\ddot{D}g\right)_{n:0}\Gamma\gamma_5 g^\dagger_{n:0}\gamma_5\Gamma^\dagger\right]\right\rangle \\ &- 2\mathrm{Re}\left\langle\mathrm{Tr}\left[\left(g\dot{D}g\right)_{n:0}\Gamma\gamma_5\left(g\dot{D}g\right)^\dagger_{n:0}\gamma_5\Gamma^\dagger\right]\right\rangle \\ &+ 8\left\langle\mathrm{ImTr}\left[\left(g\dot{D}g\right)_{n:0}\Gamma\gamma_5 g^\dagger_{n:0}\gamma_5\Gamma^\dagger\right]\mathrm{ImTr}\left[\dot{D}g\right]\right\rangle \\ &+ 2\mathrm{Re}\left\{\left\langle\mathrm{Tr}\left[g_{n:0}\Gamma\gamma_5 g^\dagger_{n:0}\gamma_5\Gamma^\dagger\right]\left(\mathrm{Tr}\left[\ddot{D}g\right] - \mathrm{Tr}\left[\dot{D}g\dot{D}g\right] + 2\mathrm{Tr}\left[\dot{D}g\right]^2\right)\right\rangle\right. \\ &- \left.\left\langle\mathrm{Tr}\left[g_{n:0}\Gamma\gamma_5 g^\dagger_{n:0}\gamma_5\Gamma^\dagger\right]\right\rangle\left\langle\mathrm{Tr}\left[\ddot{D}g\right] - \mathrm{Tr}\left[\dot{D}g\dot{D}g\right] + 2\mathrm{Tr}\left[\dot{D}g\right]^2\right\rangle\right\}.\end{aligned} \tag{B.1.10}$$

B.1.2 Response for chiral condensate

For response of the isoscalar chemical potential, using Eq. (2.2.1), we consider trace of fermion propagator

$$G = \frac{1}{2}\left\{\mathrm{Tr}\left[g\left(\hat{\mu}_u\right)\right] + \mathrm{Tr}\left[g\left(\hat{\mu}_d\right)\right]\right\} = \mathrm{Tr}\left[g\left(\hat{\mu}_S\right)\right] \quad . \tag{B.1.11}$$

At $\hat{\mu}_S = 0$ the first and the second derivative are

$$\begin{aligned} \dot{G} &= -\mathrm{Tr}\left[g\dot{D}g\right] \\ \ddot{G} &= -\mathrm{Tr}\left[g\ddot{D}g\right] + 2\mathrm{Tr}\left[g\dot{D}g\dot{D}g\right] \quad . \end{aligned} \tag{B.1.12}$$

Combining Eq.(3.1.2), Eq.(3.1.3), Eq.(B.1.9), Eq.(B.1.12) and Eq.(B.1.13) we have

$$\frac{\partial}{\partial\hat{\mu}}\mathrm{Re}\langle G\rangle = 0 \tag{B.1.13}$$

and

$$\begin{aligned} \frac{\partial^2}{\partial\hat{\mu}^2}\mathrm{Re}\langle G\rangle &= 2\mathrm{Re}\left\langle \mathrm{Tr}\left[g\dot{D}g\dot{D}g)\right]\right\rangle - \mathrm{Re}\langle\mathrm{Tr}\left[g\ddot{D}g\right]\right\rangle \\ &+ 4\left\langle \mathrm{ImTr}\left[g\dot{D}g\right]\mathrm{ImTr}\left[\dot{D}g\right]\right\rangle \\ &+ \left\langle \mathrm{ReTr}\left[g\right]\circ\left(2\mathrm{ReTr}\left[\ddot{D}g\right] - 2\mathrm{ReTr}\left[\dot{D}g\dot{D}g\right] - 4\left\{\mathrm{ImTr}\left[\dot{D}g\right]\right\}^2\right)\right\rangle_{cc} . \end{aligned} \tag{B.1.14}$$

Appendix C

C.1 Formulas for the isovector chemical potential response

C.1.1 Response for hadron masses

Next, we consider responses to the isovector chemical potential. They are given by using Eq.(2.3.1). In this case, the first derivative of Δ vanishes,

$$\dot{\Delta} = \frac{\partial}{\partial \hat{\mu}_V} \left[\det(D(\hat{\mu}_V)) \det(D(-\hat{\mu}_V)) \right] |_{\hat{\mu}_V=0} = 0 \quad , \tag{C.1.1}$$

and the second derivative is obtained as

$$\frac{\ddot{\Delta}}{\Delta} = 2\mathrm{Tr}\left[\ddot{D}g\right] - 2\mathrm{Tr}\left[\dot{D}g\dot{D}g\right] \quad . \tag{C.1.2}$$

Similarly, derivatives of G are calculated as

$$\dot{G} = -2\mathrm{ReTr}\left[\left(g\dot{D}g\right)_{n:0} \Gamma\gamma_5 g^\dagger_{n:0}\gamma_5\Gamma^\dagger\right] \quad , \tag{C.1.3}$$

and

$$\begin{aligned} \ddot{G} &= 4\mathrm{ReTr}\left[\left(g\dot{D}g\dot{D}g\right)_{n:0} \Gamma\gamma_5 g^\dagger_{n:0}\gamma_5\Gamma^\dagger\right] \\ &- 2\mathrm{ReTr}\left[\left(g\ddot{D}g\right)_{n:0} \Gamma\gamma_5 g^\dagger_{n:0}\gamma_5\Gamma^\dagger\right] + 2\mathrm{Tr}\left[\left(g\dot{D}g\right)_{n:0} \Gamma\gamma_5 \left(g\dot{D}g\right)^\dagger_{n:0} \gamma_5\Gamma^\dagger\right] \quad . \end{aligned} \tag{C.1.4}$$

Resultant expressions for the first and second responses to the isovector chemical are

$$\frac{\partial}{\partial\hat{\mu}}\mathrm{Re}\langle H(n)H(0)^\dagger\rangle = -2\mathrm{ReTr}\left[\left(g\dot{D}g\right)_{n:0} \Gamma\gamma_5 g^\dagger_{n:0}\gamma_5\Gamma^\dagger\right] \quad , \tag{C.1.5}$$

and

$$\frac{\partial^2}{\partial\hat{\mu}^2}\mathrm{Re}\langle H(n)H(0)^\dagger\rangle = 4\mathrm{Re}\left\langle \mathrm{Tr}\left[\left(g\dot{D}g\dot{D}g\right)_{n:0} \Gamma\gamma_5 g^\dagger_{n:0}\gamma_5\Gamma^\dagger\right]\right\rangle \tag{C.1.6}$$

$$
\begin{aligned}
- \quad & 2\mathrm{Re}\left\langle \mathrm{Tr}\left[\left(g\ddot{D}g\right)_{n:0}\Gamma\gamma_5 g^{\dagger}_{n:0}\gamma_5\Gamma^{\dagger}\right]\right\rangle \\
+ \quad & 2\mathrm{Re}\left\langle \mathrm{Tr}\left[\left(g\dot{D}g\right)_{n:0}\Gamma\gamma_5 (g\dot{D}g)^{\dagger}_{n:0}\gamma_5\Gamma^{\dagger}\right]\right\rangle \\
+ \quad & 2\mathrm{Re}\left\{\left\langle \mathrm{Tr}\left[g_{n:0}\Gamma\gamma_5 g^{\dagger}_{n:0}\gamma_5\Gamma^{\dagger}\right]\left(\mathrm{Tr}\left[\ddot{D}g\right]-\mathrm{Tr}\left[\dot{D}g\dot{D}g\right]\right)\right\rangle \right. \\
- \quad & \left.\left\langle \mathrm{Tr}\left[g_{n:0}\Gamma\gamma_5 g^{\dagger}_{n:0}\gamma_5\Gamma^{\dagger}\right]\right\rangle\left\langle \mathrm{Tr}\left[\ddot{D}g\right]-\mathrm{Tr}\left[\dot{D}g\dot{D}g\right]\right\rangle\right\} \quad .
\end{aligned}
$$

C.1.2 Response for chiral condensate

Since isovector chemical potential is definited by Eq. (2.3.1), the trace of fermion propagator is

$$
G=\frac{1}{2}\left\{\mathrm{Tr}\left[g(\hat{\mu}_u)\right]+\mathrm{Tr}\left[g\left(\hat{\mu}_d\right)\right]\right\}=\frac{1}{2}\{\mathrm{Tr}[g(\hat{\mu})]+\mathrm{Tr}[g(-\hat{\mu})]\}. \tag{C.1.7}
$$

Similarly, derivatives of G are calculated as

$$
\dot{G} \quad = \quad 0 \tag{C.1.8}
$$

,

$$
\ddot{G} \quad = \quad -\mathrm{Tr}\left[g\ddot{D}g\right]+2\mathrm{Tr}\left[g\dot{D}g\dot{D}g\right] \quad . \tag{C.1.9}
$$

Combining Eq.(3.1.2), Eq.(3.1.3), Eq.(C.1.1), Eq.(C.1.2) Eq.(C.1.8) and Eq.(C.1.9) we have

$$
\frac{\partial}{\partial\hat{\mu}}\mathrm{Re}\langle G\rangle=0 \tag{C.1.10}
$$

and

$$
\begin{aligned}
\frac{\partial^2}{\partial\hat{\mu}^2}\mathrm{Re}\langle G\rangle \quad &= \quad 2\mathrm{Re}\left\langle \mathrm{Tr}\left[g\dot{D}g\dot{D}g\right]\right\rangle-\mathrm{Re}\left\langle \mathrm{Tr}\left[g\ddot{D}g\right]\right\rangle \\
&+ \quad \left\langle \mathrm{ReTr}\left[g\right]\circ\left(2\mathrm{ReTr}\left[\ddot{D}g\right]-2\mathrm{ReTr}\left[\dot{D}g\dot{D}g\right]\right)\right\rangle_{cc}.
\end{aligned} \tag{C.1.11}
$$

Appendix D

D.1 Responses for staggered fermion

D.1.1 Response for hadron masses

For staggered fermion, the determinant factor Δ is given by Eq.(2.4.8), and this leads to

$$\begin{aligned} \frac{\dot{\Delta}}{\Delta} &= \frac{1}{2}\mathrm{Tr}\left[\dot{D}g\right] \quad , \\ \frac{\ddot{\Delta}}{\Delta} &= \frac{1}{2}\mathrm{Tr}\left[\ddot{D}g\right] - \frac{1}{2}\mathrm{Tr}\left[\dot{D}g\dot{D}g\right] + \frac{1}{4}\mathrm{Tr}\left[\dot{D}g\right]^2 \quad . \end{aligned} \tag{D.1.1}$$

Using Eq.(2.4.4) and Eq.(2.4.7), final expressions for the second responses are

$$\begin{aligned} \frac{\partial^2}{\partial\hat{\mu}^2} \quad \mathrm{Re} \quad & \langle H(n)H(0)^\dagger\rangle = 4\mathrm{Re}\left\langle \mathrm{Tr}\left[\left(g\dot{D}g\dot{D}g\right)_{n:0} g^\dagger_{n:0}\boldsymbol{\sigma}\right]\right\rangle \\ - \quad & 2\mathrm{Re}\left\langle \mathrm{Tr}\left[\left(g\ddot{D}g\right)_{n:0} g^\dagger_{n:0}\boldsymbol{\sigma}\right]\right\rangle \\ - \quad & 2\mathrm{Re}\left\langle \mathrm{Tr}\left[\left(g\dot{D}g\right)_{n:0}\left(g\dot{D}g\right)^\dagger_{n:0}\boldsymbol{\sigma}\right]\right\rangle \\ + \quad & 2\left\langle \mathrm{ImTr}\left[\left(g\dot{D}g\right)_{n:0} g^\dagger_{n:0}\boldsymbol{\sigma}\right]\mathrm{ImTr}\left[\dot{D}g\right]\right\rangle \\ + \quad & \frac{1}{2}\mathrm{Re}\left\{\left\langle \mathrm{Tr}\left[g_{n:0}g^\dagger_{n:0}\boldsymbol{\sigma}\right]\left(\mathrm{Tr}\left[\ddot{D}g\right] - \mathrm{Tr}\left[\dot{D}g\dot{D}g\right] + \frac{1}{2}\mathrm{Tr}\left[\dot{D}g\right]^2\right)\right\rangle \right. \\ - \quad & \left.\left\langle \mathrm{Tr}\left[g_{n:0}g^\dagger_{n:0}\boldsymbol{\sigma}\right]\right\rangle\left\langle \mathrm{Tr}\left[\ddot{D}g\right] - \mathrm{Tr}\left[\dot{D}g\dot{D}g\right] + \frac{1}{2}\mathrm{Tr}\left[\dot{D}g\right]^2\right\rangle\right\} \end{aligned} \tag{D.1.2}$$

for the isoscalar chemical potential, and

$$\begin{aligned} \frac{\partial^2}{\partial\hat{\mu}^2}\mathrm{Re}\langle H(n)H(0)^\dagger\rangle &= 4\mathrm{Re}\left\langle \mathrm{Tr}\left[\left(g\dot{D}g\dot{D}g\right)_{n:0} g^\dagger_{n:0}\boldsymbol{\sigma}\right]\right\rangle \\ &- 2\mathrm{Re}\left\langle \mathrm{Tr}\left[\left(g\ddot{D}g\right)_{n:0} g^\dagger_{n:0}\boldsymbol{\sigma}\right]\right\rangle \\ &+ 2\mathrm{Re}\left\langle \mathrm{Tr}\left[\left(g\dot{D}g\right)_{n:0}\left(g\dot{D}g\right)^\dagger_{n:0}\boldsymbol{\sigma}\right]\right\rangle \end{aligned} \tag{D.1.3}$$

$$
\begin{aligned}
&+ \quad \frac{1}{2}\mathrm{Re}\left\{\left\langle \mathrm{Tr}\left[g_{n:0}g^{\dagger}_{n:0}\boldsymbol{\sigma}\right]\left(\mathrm{Tr}\left[\ddot{D}g\right]-\mathrm{Tr}\left[\dot{D}g\dot{D}g\right]\right)\right\rangle\right. \\
&- \quad \left.\left\langle \mathrm{Tr}\left[g_{n:0}g^{\dagger}_{n:0}\boldsymbol{\sigma}\right]\right\rangle\left\langle \mathrm{Tr}\left[\ddot{D}g\right]-\mathrm{Tr}\left[\dot{D}g\dot{D}g\right]\right\rangle\right\}
\end{aligned}
$$

for the isovector chemical potential.

D.1.2 Response for chiral condensate

We use Eq.(D.1.2) for staggered fermion. Resultant expressions for the second order response of chiral condensate to chemical potential are

$$
\begin{aligned}
\frac{\partial^2}{\partial\hat{\mu}^2}\mathrm{Re}\langle G\rangle &= 2\mathrm{Re}\left\langle \mathrm{Tr}\left[g\dot{D}g\dot{D}g\right]\right\rangle - \mathrm{Re}\langle\mathrm{Tr}\left[g\ddot{D}g\right]\right\rangle \qquad \text{(D.1.4)}\\
&+ \left\langle \mathrm{ImTr}\left[g\dot{D}g\right]\mathrm{ImTr}\left[\dot{D}g\right]\right\rangle \\
&+ \left\langle \mathrm{ReTr}\left[g\right]\circ\frac{1}{2}\left(\mathrm{ReTr}\left[\ddot{D}g\right]-\mathrm{ReTr}\left[\dot{D}g\dot{D}g)\right]-\left\{\mathrm{ImTr}\left[\dot{D}g\right]\right\}^2\right)\right\rangle_{cc}
\end{aligned}
$$

for isoscalar chemical potential, and

$$
\begin{aligned}
\frac{\partial^2}{\partial\hat{\mu}^2}\mathrm{Re}\langle G\rangle &= 2\mathrm{Re}\left\langle \mathrm{Tr}\left[g\dot{D}g\dot{D}g\right]\right\rangle - \mathrm{Re}\left\langle \mathrm{Tr}\left[g\ddot{D}g\right]\right\rangle \qquad \text{(D.1.5)}\\
&+ \left\langle \mathrm{ReTr}\left[g\right]\circ\frac{1}{2}\left(\mathrm{ReTr}\left[\ddot{D}g\right]-\mathrm{ReTr}\left[\dot{D}g\dot{D}g\right]\right)\right\rangle_{cc}
\end{aligned}
$$

for isovector chemical potential.

Appendix E

To evaluate the traces in this study, we use a stochastic estimation with the Gaussian noise [43, 44]. Here, we employ the Z_2 noise method [35]. For example, Tr $\left[\dot{D}g\right]$ is written as

$$\mathrm{Tr}\left[\dot{D}g\right] = \frac{1}{N_{noise}} \sum_{i=1}^{N_{noise}} R_i^\dagger(x)\dot{D}(x,y)g(y,z)R_i(z) \tag{E.0.1}$$

with the randomly generated noise vector $R(x)_i \in \{1, -1\}$. In this representation, gR is obtained by solving a linear equation $Dx = R$ for x with a source vector R. Multiplying $\dot{D}$ and contraction with $R^\dagger$ are easy, and finally statistical average over R_i eliminates the off diagonal contributions of $\dot{D}g$ so as to evaluate the trace. The number of sample noise vectors, N_{noise} is chosen so that the statistical error concerning this trace operation must be sufficiently reduced. In this study we choose $N_{noise} = 200$.

In the Fig. E.1,we plot $\langle\bar{\psi}\psi\rangle$ which measures $\langle\bar{\psi}\psi\rangle$ as a function of noise vectors for $ma = 0.025$, $\beta = 5.29$. We measure noise vectors from 10 to 200, and configurations from 100 to 600. We find $\langle\bar{\psi}\psi\rangle$ depends on numbers of configuration, but it does not strongly depend on the number of noise vectors when the noise vectors are larger than 10. For studying the behavior of $\langle\bar{\psi}\psi\rangle$, we can choose the noise vectors as 10. However, in this study, we must also measure the other quantities, for example, Tr $\left[\dot{D}g\right]$, Tr $\left[\ddot{D}g\right]$, Tr $\left[g\dot{D}g\right]$, Tr $\left[g\dot{D}g\dot{D}g\right]$ and Tr $\left[\dot{D}g\dot{D}g\right]$, to find the relation with noise vectors. In Fig E.2 - Fig. E.6, we plot them. We find. for example, Im $\left(\mathrm{Tr}\left[g\dot{D}g\right]\right)$ (Fig. E.6) is stable when the number of noise vectors is larger than 100, and that of configurations are 600. We think 200 noise vectors are enough for this study.

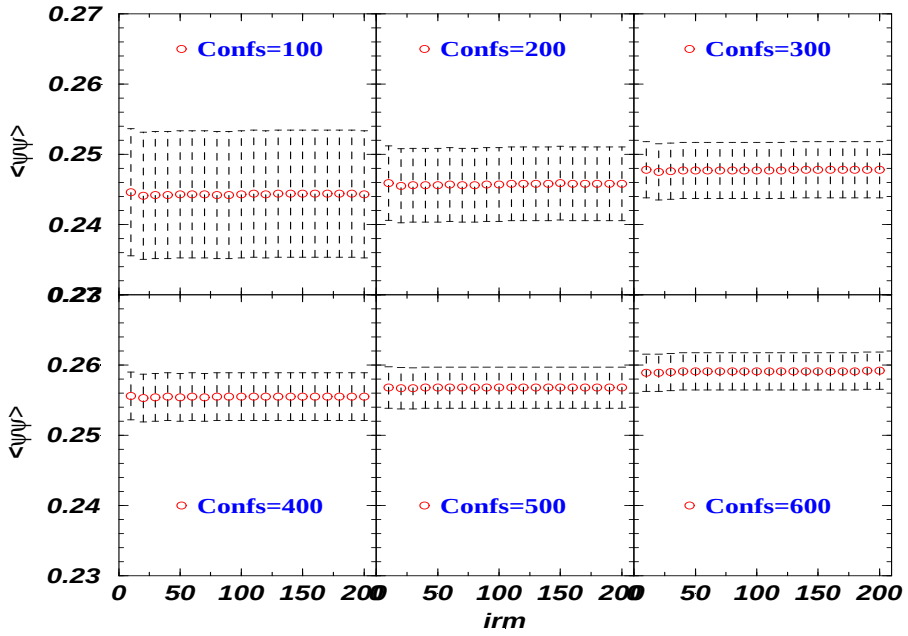

Figure E.1: $\langle\bar{\psi}\psi\rangle$ as a function of noise vectors (irm). $Confs$ denotes number of configurations. $ma = 0.025$, $\beta = 5.29$.

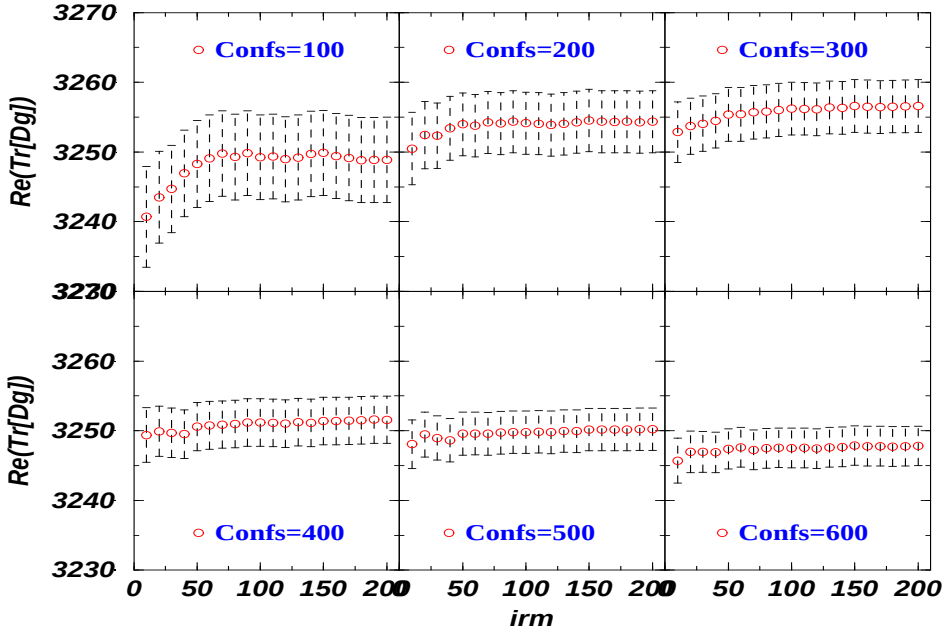

Figure E.2: Re $\left(\mathrm{Tr}\left[\ddot{D}g\right]\right)$ as a function of noise vectors (irm). $Confs$ denotes number of configurations. $ma = 0.025$, $\beta = 5.29$.

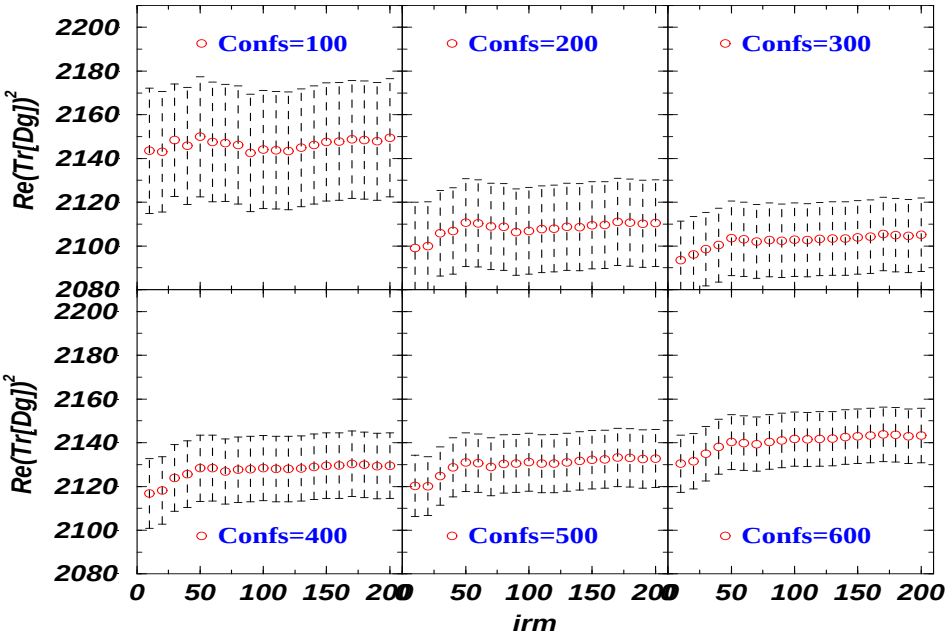

Figure E.3: Re $\left(\mathrm{Tr}\left[\dot{D}g\right]\right)^2$ as a function of noise vectors (irm). $Confs$ denotes number of configurations. $ma = 0.025$, $\beta = 5.29$.

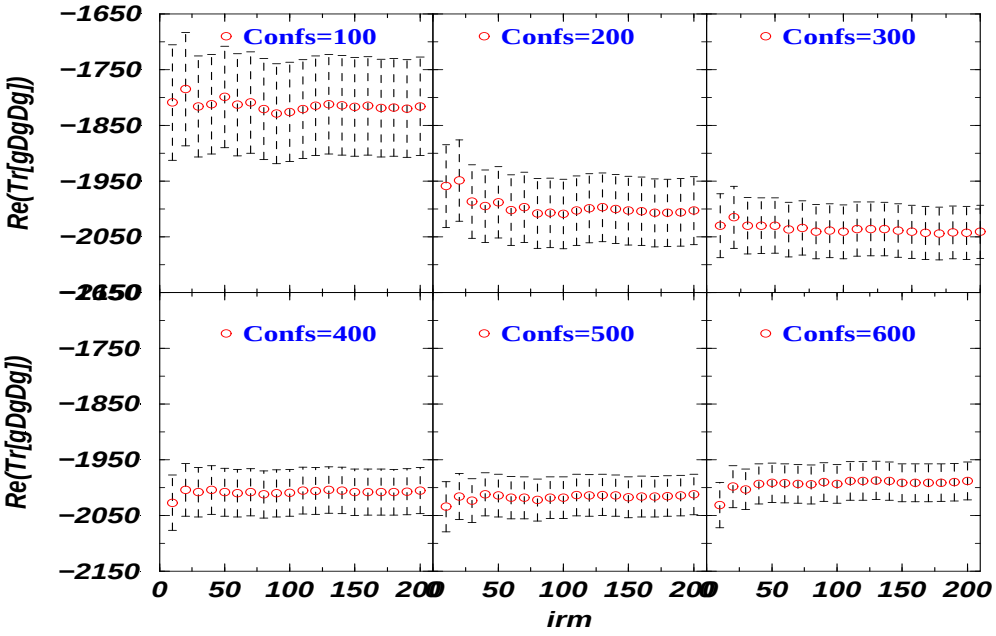

Figure E.4: Re $\left(\mathrm{Tr}\left[g\dot{D}g\dot{D}g\right]\right)$ as a function of noise vectors (irm). $Confs$ denotes number of configurations. $ma = 0.025$, $\beta = 5.29$.

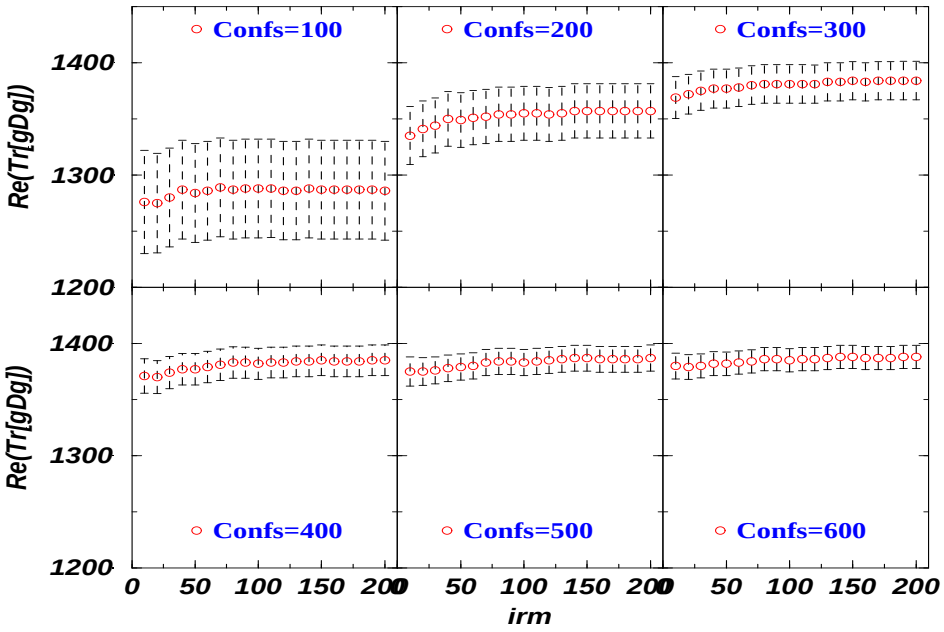

Figure E.5: Re $\left(\mathrm{Tr}\left[g\ddot{D}g\right]\right)$ as a function of noise vectors (irm). $Confs$ denotes number of configurations. $ma = 0.025$, $\beta = 5.29$.

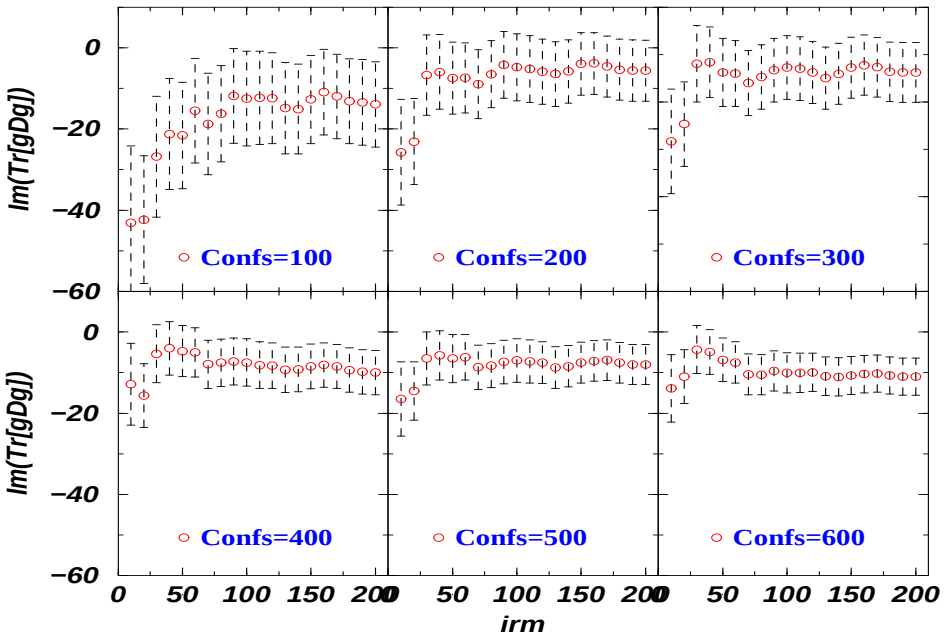

Figure E.6: Im $\left(\mathrm{Tr}\left[g\dot{D}g\right]\right)$ as a function of noise vecotrs (irm). $Confs$ denotes number of configurations. $ma = 0.025$, $\beta = 5.29$.

Bibliography

[1] M. Alford, K. Rajagopal, and F. Wilczek, Phys. Lett. B **422**, 247 (1998).

[2] R. Rapp, *et al.,* Phys. Rev. Lett. **81**, 53 (1998).

[3] K. G. Wilson, Phys. Rev. D **10**, 2445 (1974).

[4] M. Creutz, Phys. Rev. D **21**, 2308 (1980).

[5] S. Muroya, A. Nakmura, and C. Nonaka, Nucl. Phys. B **(Proc. Suppl.) 94**, 469 (2001).

[6] A. Nakamura, Phys. Lett. B **149**, 391 (1984).

[7] M. A. Stephanov, Phys. Rev. Lett. **76**, 4472 (1996).

[8] T. Hatsuda and S. H. Lee, Phys. Rev. C **46**, R34 (1992).

[9] A. Hayashigaki, Phys. Lett. B **487**, 96 (2000).

[10] CERES collaboration : G. Agakishev *et al.*, Nucl. Phys. A **638**, 159 (1998).

[11] NA50 collaboration : M. C. Abreu *et al.*, Phys. Lett. B **477**, 28 (2000).

[12] NA50 collaboration : M. C. Abreu *et al.*, Nucl. Phys. B **(Proc. Suppl.) 94**, 204 (2001).

[13] R. Rapp and C. Gale, Phys. Rev. C **60**, 024903 (1999);

[14] J. Stachel, Nucl. Phys. A **654**, 119C (1999);

[15] R. Rapp and J. Wambach, *nucl-th/0001014.*

[16] I. M. Barbour, *et al.,* Nucl. Phys. B **(Proc. Suppl.) 60A**, 220 (1998).

[17] O. Kaczemarek, *et al.,* Nucl. Phys. B **(Proc. Suppl.) 83-84**, 369 (2000).

[18] F. Karsch, Nucl. Phys. B **(Proc. Suppl.) 83-84**, 14 (2000).

[19] G. Aarts, F. Karsch, O. Kaczmarek and I.-O. Stamatescu, "1/M correction to quenched QCD with non-zero baryon density" *hep-lat/0110145.*

[20] A. Hart, M. Laine, and O. Philipsen, Phys. Lett. B **505**, 141 (2001).

[21] S. Gottlieb *et al.*, Phys. Rev. D **38**, 2888 (1988).

[22] S. Gottlieb *et al.,* Phys. Rev. D **47**, 3619 (1993).

[23] S. Gottlieb *et al.,* Phys. Rev. D **55**, 6852 (1997).

[24] S. Duane and J. B. Kogut, Nucl. Phys. B **275**, 398 (1986).

[25] S. Duane, *et al.,* Phys. Lett. B **195**, 216 (1987).

[26] QCDTARO-collaboration : Ph. de Forcrand *et al.,* Nucl. Phys. B **(Proc.Suppl.) 63A-C**, 460 (1998).

[27] QCDTARO-collaboration : Ph. de Forcrand *et al.,* Nucl. Phys. B **(Proc.Suppl.) 73**, 477 (1999).

[28] QCDTARO-collaboration : S. Choe *et al.,* "Responses of hadrons to the chemical potential at finite temperature" contribution to *Quark matter 2001.*

[29] QCDTARO-collaboration : S. Choe *et al.,* "Screening mass responses to chemical potential at finite temperature" contribution to Lattice 2001, and appear *hep-lat/0110223.*

[30] QCDTARO-collaboration : S. Choe *et al.,* "Responses of hadrons to the chemical potential at finite temperature" to be published in Phys. Rev. D **65**, 0145XX. (2002).

[31] QCDTARO-collaboration : S. Choe *et al.,* Nucl. Phys. A **698**, 395 (2002).

[32] D. T. Son and M. A. Stephanov, Phys. Rev. Lett. **86**, 592 (2001).

[33] M. Fukugita *et al.*, Phys. Rev. D **42**, 2936 (1990).

[34] S. Gottlieb *et al.*, Phys. Rev. D **35**, 3972 (1987).

[35] S. J. Dong and K. F. Liu Phys. Lett. B **328**, 130 (1994).

[36] CP-PACS Collaboration : A. Ali *et al.,* Phys. Rev. D **64**, 074510 (2001).

[37] P. Hasenfratz, F. Karsch Phys. Lett. B **125**, 308 (1983)

[38] J. Kogut,*et al.,* Nucl. Phys. B **225**, 93 (1983)

[39] N. Bilic, R.V. Gavai, Z. Phys. C **23**, 77 (1984).

[40] R.V. Gavai, Phys. Rev. D **32**, 519 (1985).

[41] J. Engles, *et al.,* Phys. Lett. B **252**, 625 (1990).

[42] D. Toussaint, Nucl. Phys. B **(proc. Suppl.) 17**, 248 (1990).

[43] K. Bitar, *et al.,* Nucl. Phys. B **313**, 348 (1989).

[44] H. R. Fiebig and R. M. Woloshyn, Phys. Rev. D **42**, 3520 (1990).